Review

Recent Progress of Electrically Pumped AlGaN Diode Lasers in the UV-B and -C Bands

Syed M. N. Hasan, Weicheng You, Md Saiful Islam Sumon and Shamsul Arafin *

Department of Electrical and Computer Engineering, The Ohio State University, Columbus, OH 43210, USA; najibhasan.1@osu.edu (S.M.N.H.); you.249@osu.edu (W.Y.); mdsumon1665bd@gmail.com (M.S.I.S.)
*   Correspondence: arafin.1@osu.edu

Abstract: The development of electrically pumped semiconductor diode lasers emitting at the ultraviolet (UV)-B and -C spectral bands has been an active area of research over the past several years, motivated by a wide range of emerging applications. III-Nitride materials and their alloys, in particular AlGaN, are the material of choice for the development of this ultrashort-wavelength laser technology. Despite significant progress in AlGaN-based light-emitting diodes (LEDs), the technological advancement and innovation in diode lasers at these spectral bands is lagging due to several technical challenges. Here, the authors review the progress of AlGaN electrically-pumped lasers with respect to very recent achievements made by the scientific community. The devices based on both thin films and nanowires demonstrated to date will be discussed in this review. The state-of-the-art growth technologies, such as molecular beam epitaxy (MBE) and metalorganic chemical vapor deposition (MOCVD); and various foreign substrates/templates used for the laser demonstrations will be highlighted. We will also outline technical challenges associated with the laser development, which must be overcome in order to achieve a critical technological breakthrough and fully realize the potential of these lasers.

1. Introduction

The electrically pumped (EP) and continuous-wave (CW) operating AlGaN-based diode lasers in the ultraviolet (UV)-B (320–280 nm) and UV-C (280–100 nm) wavelengths have significant potential in the four major application areas: free space non-line-of-sight communications [1], sensing [2], disinfection [3–5], and biomedicine [6,7]. A compilation of all the relevant applications in each area is shown in Figure 1. More recently, light sources operating at these wavelengths are discovered to be useful for sterilization of surfaces or objects, a necessary step to fight the global spread of coronavirus disease 2019 (COVID-19) [8,9]. While arguably some of these applications could be enabled by light-emitting diodes (LEDs), a wide range of applications of these UV-LEDs are limited due to their large-size, high-cost, and energy-inefficiency. Their advanced counterparts, e.g., lasers, however, show the promise of achieving low size, weight, power, and cost (SWaP-C) enabling devices [10]. Most importantly, lasers alleviate the light extraction and efficiency-droop constraints commonly found in III-nitride LEDs and extend their applications toward disinfection to air and large-surface sterilization at standoff distances because of their high-power density and light directionality.

Owing to its extraordinary band tuning capability, ternary $Al_xGa_{1-x}N$ alloys with high to mid-range aluminum (Al) compositions are one of the most promising candidates to cover the entire UV-B and up to 206 nm of the UV-C spectral region [11]. Despite successful demonstrations of UV electroluminescence (EL) back in 1970 [12], several attempts to achieve AlGaN EP lasers failed with only reported success limited to the UV-A spectral range until 2015 [13–19]. The recent encouraging results of AlGaN optoelectronic devices

including optically-pumped (OP) lasers [20–24] suggest the promise of $Al_xGa_{1-x}N$ alloys. However, optical pumping significantly increases the complexity and cost of the overall system due to the use of an additional power-hungry pump laser. The use of AlGaN as active layers is made possible mainly due to significant efforts made in the past decades for developing low-defect density templates and high-quality epi-layers through optimized growth processes. Hence, the AlGaN material system shows great potential for realizing EP lasers emitting in the range of 206–320 nm.
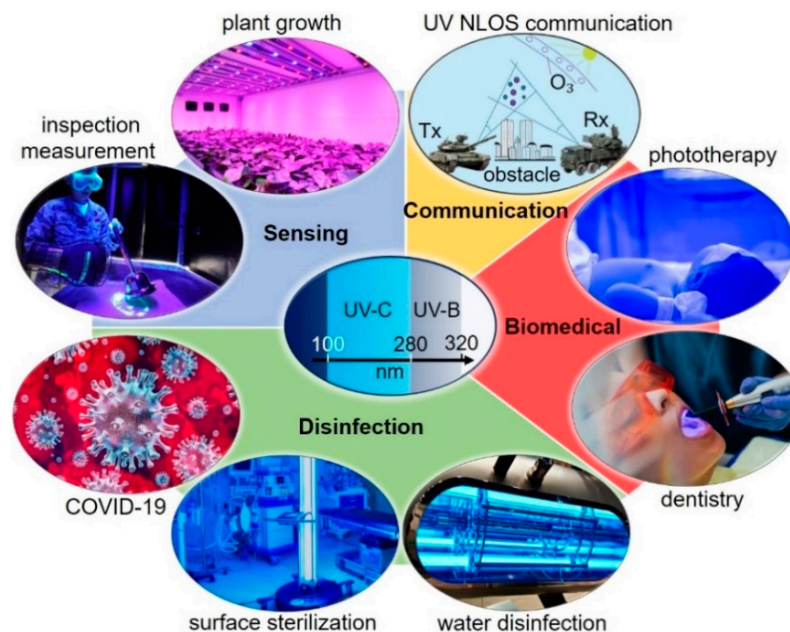

Figure 1. Overview of various applications categorized into four major areas enabled by ultraviolet (UV)-B (320–280 nm) and UV-C (280–100 nm) lasers.

From the perspective of material types, both thin films and one-dimensional nanostructures are already studied, and fascinating laser results are achieved. Since obtaining high-quality substrates to grow low-defect AlGaN epitaxial thin films has been a bottleneck for many years, nanowires (NWs) are considered to be a viable alternative to access at these wavelengths [25–29]. In 2019, the first EP thin-film UV-C laser diode was demonstrated [30]. Since then, thin film-based devices continue to show progress, sporadically covering both the UV-B and UV-C wavelengths [30–37]. Due to materials challenges and difficulties in device processing, the cavity type is still restricted to only simple Fabry–Pérot edge-emitting lasers which need to be expanded to achieve complete utilization in multipurpose applications.

NWs offer fundamental advantages over thin film-based devices because of a number of intriguing properties including the ease of NWs growth without strain [38,39]; reduction of dislocations and other structural defects; enhanced dopant incorporation [40,41] and high-quality material development by effective strain management due to a large surface-to-volume ratio [25]. Recent studies show that AlGaN NWs with N-polarity and a tailored geometry can be utilized for designing low-threshold random lasers. Interestingly, the first EP sub-300 nm top-emitting lasers were demonstrated on the NW-based platform [28]. After the first demonstration of NW-based cryogenically-cooled EP lasers emitting at UV-C [28], their room temperature (RT) operation at the UV-B range was reported [27,29,42].

Given that the newly developed AlGaN laser technology for realizing UV-B and -C lasers coincides with the rapid increase in interest for the intended applications, a comprehensive review of recent progress and research activities is of paramount importance. A brief review on AlGaN UV-LEDs [43] explained the technologies involved in developing low threading dislocation density (TDD) AlGaN on sapphire, some of which have been implemented on laser structures. A shorter review covering AlGaN UV-lasers based on

NWs with different UV wavelengths can be found in references [44,45]. Although there are book chapters and reviews on EP AlGaN lasers based on thin films [46–48] and NWs [45,49] at the broad UV band, focused reviews on such devices emitting, in particular, at the UV-B and -C spectral bands, however, are still missing. MBE-grown AlGaN thin film-based OP lasers and NW-based EP lasers emitting in the UV-C and part of UV-B (sub-300 nm) wavelengths were discussed in the very recent review [50].

Our focused review will cover only EP AlGaN lasers based on both thin films and NWs grown by either MBE or MOCVD. All the experimental efforts for realizing EP AlGaN lasers in the wavelengths covering UV-B and -C bands are summarized here. Due to the multidisciplinary nature of material growth, device design, fabrication, and characterization, we have striven to make this review accessible to individuals with varying backgrounds by giving a comprehensive overview of important aspects of AlGaN laser technology and providing details related to laser demonstrations.

We begin with a brief review of the recent developments of EP UV-B and -C laser technology in Section 2. The technical challenges associated with this UV-B and -C laser technology are then described. We then focus on the four major technical areas including substrate material, growth technology, hole injection and laser gain medium—in which dedicated effort needs to be made on in order to make a critical technological breakthrough. We next present all the laser experimental demonstrations that are reported to date as well as their relevant design, fabrication, and device characterization details. Finally, we provide concluding remarks with a general outlook for technological advancement that will pave the way for the exciting prospects of UV laser-based photonics.

2. Overview of Recent Progress of AlGaN Ultraviolet (UV)-B and -C Lasers

UV-B and -C LEDs have already successfully ensured reasonably good performance metrics. Hence, these devices are commercially available from a number of suppliers [51,52]. However, the additional complexity in terms of epi-structures [53,54], thicker layers [23,55,56] and higher crystalline quality [57–59] requirements have enabled achievement of lasers limited to only the UV-A wavelength span; which requires low-Al containing AlGaN heterostructures. For a long time until 2015, the shortest wavelengths reported for EP AlGaN-based UV lasers were 336 nm [60] and 334 nm [26] for thin films and NWs, respectively.

The first-ever sub-300 nm EP AlGaN-based thin film-based lasers with an emission wavelength of 271.8 nm was demonstrated in 2019 [30]. Only four months after the first demonstration, pulse and RT operating UV-B lasers at 298 nm were reported [31]. Similarly, in reference [33], the authors presented laser devices emitting at ~279 nm by following the epi-layer design in reference [30] with lower threshold current density. Omori et al. reported the improvement in 298 nm UV-B laser performance [32] by employing a slightly different active region. The technological advances over time for EP UV-B and -C lasers are illustrated in Figure 2.

Due to the unique ability of lateral stress relaxation associated with large surface area, developing high-quality AlGaN NWs has been quite successful with a wide range of Al compositions. In 2015, the first EP AlGaN based NW laser emitting at 262.1 nm was achieved [28]. Later in the same year, the same group demonstrated the EP AlGaN-based NW lasers, for the first time, at UV-B [27]. With further exploration, Zhao et al. reported RT operating EP AlGaN [29] based lasers at 239 nm in 2016 which, to date, is the lowest EP laser wavelength among all the thin film and NW-based devices. Table 1 provides a summary of AlGaN lasers and their corresponding performance parameters demonstrated by different research teams in the world.
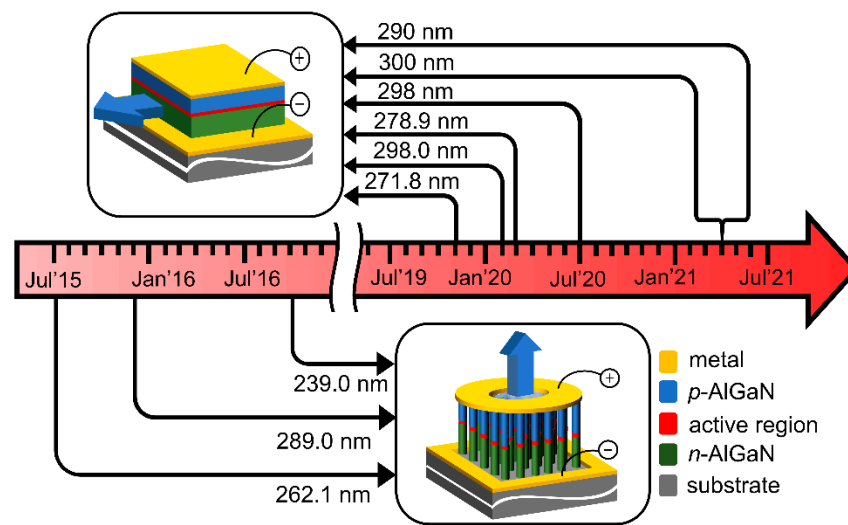
Figure 2. All key demonstrations [27–36] for electrically-pumped AlGaN lasers covering ultraviolet (UV)-B and -C wavelengths since 2015.

Table 1. A brief summary of experimental realizations of AlGaN electrically pumped (EP) lasers listed based on the material types.

Reference	Growth Method	Material Type	Lasing Wavelength (nm)	Threshold (kA/cm^2)	Substrate	Operating Temp.	Operating Mode
Zhang et al., 2019 [30]	MOCVD	Thin film	271.8	25	AlN single crystal	RT	Pulse
Sato et al., 2020 [31]	MOCVD	Thin film	298	41	AlN/sapphire	RT	Pulse
Sakai et al., 2020 [33]	MOCVD	Thin film	278.9	19.6	AlN single crystal	RT	Pulse
Omori et al., 2020 [32]	MOCVD	Thin film	298	25	AlN/sapphire	RT	Pulse
Kushimoto et al., 2021 [34]	MOCVD	Thin film	271.2		AlN single crystal	RT	Pulse
Tanaka et al., 2021 [35]	MOCVD	Thin film	300	13.3	AlN/sapphire	RT	Pulse
Tanaka et al., 2021 [36]	MOCVD	Thin film	290	35	AlN/sapphire	RT	Pulse
Zhao et al., 2015 [28]	MBE	Nanowire	262.1	0.2	Si	77K	CW
Zhao et al., 2015 [27]	MBE	Nanowire	289	0.3	Si	RT	CW
Zhao et al., 2016 [29]	MBE	Nanowire	239		Si	RT	CW

MOCVD = metalorganic chemical vapor deposition, MBE = molecular beam epitaxy, RT = room temperature, CW = continuous-wave.

3. Challenges of AlGaN UV-B/C Lasers

Despite significant development in growing single-crystalline AlGaN materials, realizing high-efficiency AlGaN-based laser diodes in the range of UV-B and -C is still challenging owing to several technical issues which are briefly described in Section 3. Figure 3 illustrates the major four challenges associated with the development of AlGaN laser technology.

3.1. Substrates and Defects

AlN templates with low dislocation density and point defects are essential to enhance the emission efficiency of UV lasers. Nearly 80 times improvement in IQE was reported for AlGaN QW grown on AlN/sapphire templates with a TDD of 5×10^8 cm^{-2} compared to those grown on conventional templates with TDDs 2×10^{10} cm^{-2} [61–63]. Due to the employment of different growth techniques such as HTA-sputtered AlN, epitaxial lateral overgrowth (ELO), patterned sapphire substrate (PSS) and thick AlN layer growth, significant advancement was made on AlN/sapphire over the years [64–67]. This led to TDDs in the range of 10^7–10^9 cm^{-2}. Using AlN bulk substrate which has a very low defect density in the range of 10^3–10^4 cm^{-2} has been quite popular for obtaining high-quality epilayers [30,68].
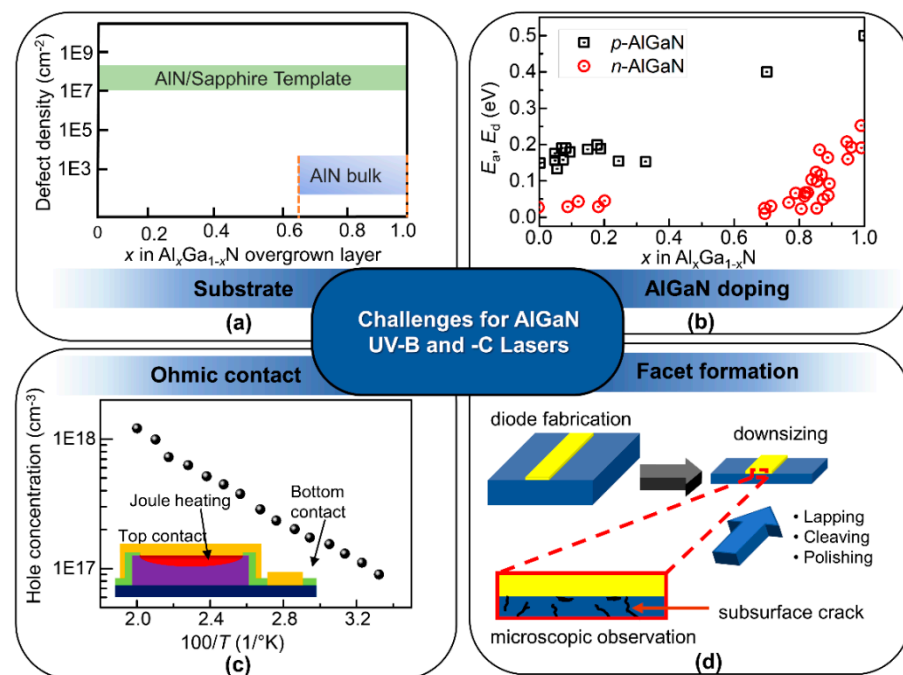
Figure 3. Four major challenges on the way towards demonstrating UV-B (320–280 nm) and UV-C (280–206 nm) lasers. (**a**) Current status of defect density in AlGaN films grown on AlN bulk substrate and AlN/sapphire template, (**b**) the change of acceptor and donor activation energy for $Al_xGa_{1-x}N$ with x [69–75], (**c**) the high temperature requirement to achieve adequate hole concentration makes it challenging to achieve low resistive ohmic contacts [76]. Joule heating effect due to high contact resistance is shown in the inset, and (**d**) subsurface crack generation during facet formation. Figure (**c**) is reproduced with permission from reference [76]. Copyright (1998) Elsevier B.V.

AlN bulk substrates developed by physical vapor transport (PVT) or hydride vapor phase epitaxy (HVPE) are now commercially available to be implemented in UV-optoelectronics [21,77–79]. However, while $Al_xGa_{1-x}N$ with any Al mole fraction x was possible to grow on AlN/sapphire templates without degrading overgrown epilayers, pseudomorphic growth on top of AlN bulk substrates with no strain relaxation was reported up to $x = 0.65$ (Figure 3a) [80,81]. Large-scale growth of AlN bulk crystal is still under development, making the substrate quite expensive. Along with the high cost, other issues such as Mg-dopant defect-related absorption, and unavailability of conducting substrates impede the UV-optoelectronics from enabling completely [78,82–84]. While AlN bulk substrates or AlN/sapphire templates are the material of choice for growing AlGaN thin films, silicon is usually used in growing high-quality AlGaN NWs. The potential solutions to overcome the challenges regarding high-quality substrates and low-defect templates are presented in detail in Sections 4.1 and 4.2.

3.2. P- and N-Doping for High-Al

As UV-B and -C lasers require high-quality, low-defect and thick AlGaN cladding layers for improved waveguiding [24,85], their electrical performance is equally important. To achieve the high current density required in the active regions for laser operation, cladding layers need to be conductive which is particularly challenging for *p*-type doping for all x of $Al_xGa_{1-x}N$, as shown in Figure 3b [72]. Behind ineffective *p*-doping, the most formidable challenges include large acceptor ionization energy for Mg dopants in AlGaN [86,87], formation of low energies by compensating defects (donors) like nitrogen vacancies [88], limitation of solubility of Mg in AlGaN [71,89], hydrogen passivation of the Mg dopants [70,90] and the existence of parasitic impurities, such as hydrogen (H), carbon (C) and oxygen (O) [69,91,92]. While significant efforts were made to develop low-defect, highly p-doped AlGaN layers using AlN bulk substrate and engineered sapphire templates,

approaches such as distributed polarization doping (DPD), short-period superlattice (SPSL) and tunnel junction (TJ) will bypass the *p*-doping problem. A brief discussion on these three approaches can be found in Section 4.3.

Compared to *p*-type doping, *n*-type doping is easily attainable and Si-doped AlGaN up to $x = 0.8$ with a reasonable doping concentration was achieved [73–75]. However, a sharp increase in resistance was observed due to the high activation energy of Si which increases exponentially from 25 meV–250 meV once the $x > 0.8$ for n-Al$_x$Ga$_{1-x}$N [73]. On top of this, the presence of compensating impurities carbon and oxygen in AlN substrates as well as MOCVD reactor impurities decrease donor concentrations in AlGaN with $x > 0.85$ by an order of magnitude [68,91,93].

3.3. Low-Resistive Ohmic Contact

High-doping concentrations in both *n*- and *p*-contact layers are usually required to form low-resistive ohmic contacts for current injection [94,95]. However, it becomes challenging for AlGaN materials due to the aforementioned reasons. At a nearly degenerately doping level, a "knee behavior" in conductivity due to self-compensation (vacancy-silicon complexes in *n*-type and nitrogen vacancies in *p*-type) appears [82]. A common practice is to grow a degenerately-doped GaN layer to make ohmic contacts, which requires linear Al compositional grading down to $x = 0$ [96,97]. Due to the use of insulating substrates, large-area backside n-contact formation is not possible. Figure 3c shows the representative AlGaN lasers with co-planar or intracavity contacts, which is the only possible way to form bottom *n*-side contacts. As the improvement in *n*- and *p*-type conductivity in Al-rich AlGaN continues, the low resistive ohmic contact realization emerges. As development continues in *n*- and *p*-type doping in AlGaN layers, as discussed in Sections 3.2 and 4.3, the low resistive ohmic contact realization emerges.

3.4. Facet Formation

Unlike the other III–V compound semiconductor-based lasers, III-nitride materials provide a reflectivity of only ~19% from the naturally cleaved facet at the semiconductor–air interface. This may necessitate a high-reflection coating on one of the facets in order to overcome resonator losses and obtain lasing, as schematically shown in Figure 3d. Another issue is that both sapphire and AlN are extremely hard materials. Hence, backend processes including substrate lapping and laser scribing to obtain mirror-finish facets pose many technical challenges to complete laser fabrication [98,99]. One sometimes breaks processed lasers and polishes the cavity-ends to obtain high-quality facets, which, however, increases manufacturing cost.

4. Critical Technical Areas for AlGaN UV-B and -C Lasers

A great deal of research has been devoted to achieving technical knowledge on the way towards overcoming the challenges mentioned in Section 3. When it comes to EP laser technology development, good cavity design is one of the first steps. Good device performance can be obtained by an optimized laser heterostructure design, such as choosing layer thicknesses and compositions, as well as separate confinement heterostructures with strong transverse mode confinement to maximize the overlap with AlGaN QWs. This has to be combined with reducing the optical losses in EP lasers which is particularly challenging due to absorption tails in the highly Mg-doped *p*-AlGaN cladding and waveguide layers. A number of reviews, regular papers, and book chapters already provided a comprehensive discussion of this important aspect for both UV-B [100,101] and -C [24,46,54,102–105]. Therefore, we have considered this discussion in our review paper to be redundant. Instead, this review aims to capture some of the critical technical aspects that are not well-addressed in the literature. Figure 4 schematically shows the four major technical pillars that will determine the success of UV-B and -C laser technology and underpin the implementation of high-performance AlGaN devices.
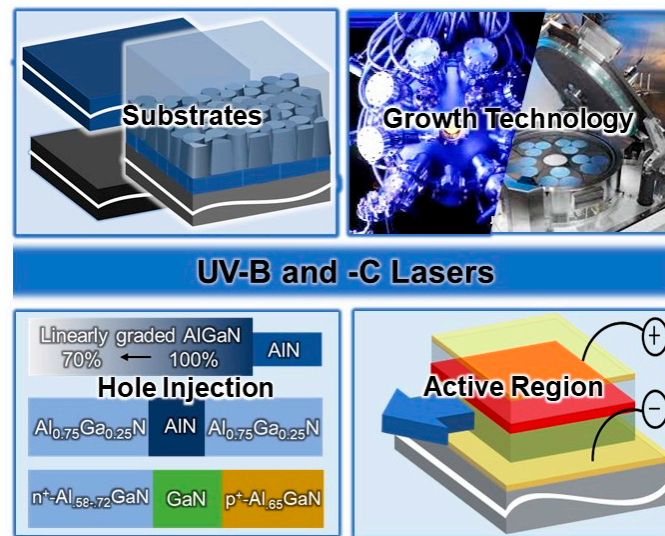
Figure 4. Major technical pillars determining the success of UV-B and UV-C laser technology.

4.1. Substrate Materials

The most commonly used two substrate materials for the growth of AlGaN laser epilayers are bulk AlN crystal substrates, and MOCVD-grown AlN templates on sapphire. For NW-based lasers, silicon is one of the most popular substrate materials. Though AlN bulk substrates offer low TDD, their use is still limited to fabricating high-cost devices and rarely considered for commercial applications. Figure 5 schematically shows all the possible substrates that are used for implementing EP AlGaN lasers. Unlike GaAs or Si, bulk nitrides cannot be grown using the conventional Czochraslski or Bridgman techniques because of their high melting temperature and very high dissociation pressure [106–108]. To develop AlN substrate with low dislocation either PVT/sublimation technique [109,110] or HVPE [111,112] is employed. Despite the successful demonstration of growing low TDD AlGaN layers on top of AlN substrates [80,113], the use of AlN buffer templates grown on top of sapphire is still the most popular way of growing AlGaN based LEDs and lasers as well as other electronic devices.
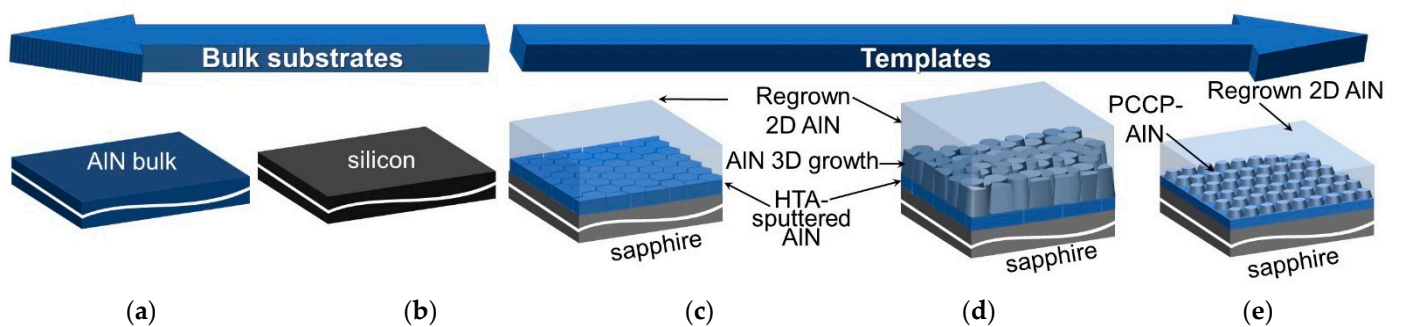

Figure 5. Possible substrate options for thin film and NW-based full UV-B (320–280 nm) and partial UV-C (280–206 nm) lasers. (**a**,**b**) represents the bulk substrates AlN and Si, respectively. (**c**) schematically shows the AlGaN thin film samples grown on HTA-AlN template. (**d**,**e**) demonstrates newly developed two-step growth templates with self-nucleating 3D AlN growth and periodic concavo-convex pattern AlN, respectively.

4.1.1. Substrates for UV-C Lasers

Conventionally UV-C AlGaN based devices are realized on AlN bulk substrates without templates. Pseudomorphic growth of doped or undoped AlGaN layers with >60% Al content [82,114] on AlN substrates have been possible with dislocation density less than 10^3 cm^{-2}, being over-qualified for making EP lasers. The AlN bulk crystal substrate cost

largely varies with the amount of dislocation density. With a substrate with $<10^3$ cm^{-2} dislocation density, wafer costs exceeds over $5 K. A list of commercially available AlN substrates and AlN/sapphire template with their respective cost and selling companies is given in Table 2.

Table 2. Different companies selling commercial AlN substrates and AlN/sapphire templates.

Company	Cost/cm^2	Dislocation Density (cm^{-2})	Largest Available Wafer Dimension	Substrate
Hexatech [115]	$275	$<1 \times 10^3$	5.08 cm dia	Bulk crystal
MTI Corporation [116]	$1995	$<1 \times 10^5$	1 cm × 1 cm	Bulk crystal
Kymatech [117]	$18	Threading 5×10^8	5.08 cm dia	AlN/sapphire
MSE supply [118]	$22	Screw 5.5×10^7 Edge 1.8×10^9	5.08 cm dia	AlN/sapphire
MTI Corporation [119]	$5		10.16 cm dia	AlN/sapphire

In spite of the high cost, bulk AlN crystal is still the material for choice for realizing UV-C lasers. To our best knowledge, all the EP UV-C lasers experimentally realized so far used materials that were grown on AlN bulk substrates by leveraging its low dislocation density property. It should be noted that substrate contributes only 10–20% of the overall cost in UV lasers or LEDs [120], thus solving the issues regarding active region optimization, *p*-AlGaN contacts should receive much more attention.

4.1.2. Substrates for UV-B Lasers

To grow AlGaN lasers suitable for UV-B applications, it was found that strain relaxation is inevitable due to the large lattice mismatch between AlN and AlGaN. AlGaN layers with 55% Al composition on top of both AlN bulk crystal and AlN/sapphire were successfully grown and no clear dependence on substrates was found when the thickness of AlGaN layers was >5 μm [23,31]. A high-temperature annealing (HTA) process at any thickness of the initially deposited AlN by sputtering was found to result in an order of reduction in dislocation density compared to non-annealed AlN thin films [121]. The HTA process of thin AlN layers to reduce TDD is a relatively new process [122–124], and subsequent continuous growth of AlN at a relatively high temperature followed by AlGaN growth with appropriate Al composition by MOCVD for laser epilayers was undertaken.

The 3D schematic of the HTA-sputtered AlN/regrown AlN templates is shown in Figure 5c. Such templates help bend TDDs while annealing, which was one of the keys to obtaining high-quality AlGaN active epilayers for EP lasers [31,124]. Soon after, transferring from direct 2D growth on top of the HTA AlN layer to a two-step growth method was reported. In the two-step method, 3D growth was first initiated on top of the HTA AlN layer prior to proceeding to 2D growth, as shown in Figure 5d. The dislocation density was significantly reduced in this novel growth technique [23]. While both templates were successful in terms of EP laser demonstrations in the UV-B range [31,32], the templates shown in Figure 5d are preferred. Very recently, another innovative two-step growth method has been reported [36]. Instead of using self-nucleated 3D AlN, patterned growth was employed in this novel technique where AlN films were first turned into a 3D periodic plano cocavo-convex patterns (PCCPs) as schematically shown in Figure 5e. However, the early stage demonstration of the process produced templates with a higher defect density compared to the self-nucleated 3D growth templates (see Figure 5d) and the resulting UV-B lasers of poorer performance.

4.1.3. Silicon Substrates for Nanowire Lasers

The development of AlGaN-based NWs grown on Si was largely influenced due to the large demand of Si photonics. With three-fold atomic symmetry (triangular lattice),

Si (111) surface can grow AlGaN wurtzite crystal structures with an epitaxial relation to it [26,125–128]. Growing high-quality NWs on top of highly-desired CMOS-compatible Si (100) still remains a challenge and this area experienced very limited success [129,130].

4.2. Growth Technology

The two most popular methods available for epitaxial growth AlGaN UV laser materials are molecular beam epitaxy (MBE) [128,131–133] and metalorganic chemical vapor deposition (MOCVD) [134–136]. When it comes to templated substrates, MOCVD is superior to MBE for growing high-quality AlN templates due to high growth-temperatures and -rates [137–139]. One can then grow laser materials by employing either of the growth techniques on top of such MOCVD-grown templates. MOCVD-grown AlGaN QW UV-C LEDs with 10–20% EQE [62,97,140] and IQE as high as 85% [141] were achieved. Considering OP lasers [102,142], and very recent demonstrations of EP lasers at both UV-B [31] and -C [30], MOCVD has been the most popular choice mostly due to its wide growth window in terms of various growth parameters.

Although not as extensive as MOCVD, MBE-grown UV materials, i.e., both thin film and NWs, have also been studied over the years. As a matter of fact, MBE offers some distinct benefits over MOCVD in terms of interface diffusion, defect control, memory effect, high hole concentration in p-AlGaN, Mg passivation and significant control over defect incorporation [143]. Due to its relatively low growth temperature MBE grown samples do not suffer from surface damage due to chemical reaction at high temperature often associated with MOCVD. This suggests the superiority of MBE over MOCVD in terms of growing high-quality active regions. Noticeable success in terms of implementing EP UV-C lasers using, in fact, NWs was achieved [144–146]. In MBE, AlGaN NWs are typically grown spontaneously in N-rich conditions on Si substrate with GaN NW template grown over it.

Lasers with buried TJ may require a hybrid MOCVD/MBE growth approach [147,148]. In such structures, a base structure, containing all the layers up to an active region and the p^+-side of the TJ, is grown by MOCVD, and the remainder of the device including the n^+-side of TJs, n-cladding and n^+-contact layers can be overgrown during the second epitaxial growth by MBE. Hence, the hybrid approach, comprising a MOCVD-grown base structure with the active region and MBE-grown TJs, is another viable alternative towards obtaining high-performance UV-B and -C lasers. As a matter of fact, the MOCVD-grown TJs are found to be more resistive compared to the MBE-grown equivalent structures [149–151]. Thus, growing the samples in two growth steps involves a tradeoff between the process complexity/device cost and attainable device performance.

4.3. Three Major Techniques for Hole Injection

In addition to the substrates issue, poor hole injection into active regions and the resulting reduced optical efficiency is another critical area of research. Low achievable doping for p-AlGaN cladding layers has been the fundamental roadblock to this problem. Extensive efforts are underway to improve p-type doping in AlGaN alloys. Using heavily-doped low-bandgap and non-transparent p-GaN as contact layers on top of thick p-AlGaN cladding circumvent the problem of the formation of low-resistive ohmic contacts. However, it comes at the expense of growing complex graded compositional profiles. Note that low light extraction efficiency in LEDs due to the high absorption nature of p-GaN at the UV spectral range is not a concern for resonant device like lasers [152]. In this section, we review the three state-of-the-art approaches to alleviate the p-AlGaN doping issue for implementing all-AlGaN EP lasers. We also emphasize their suitability to be adopted in different structures that translates improved device performance.

4.3.1. Distributed Polarization Doping

Introducing dopants in AlGaN by compositionally grading, commonly addressed as DPD takes advantage of both spontaneous and piezoelectric polarization. Since its first

demonstration, DPD has been widely popular as an effective means to enhance *p*-AlGaN doping [153]. In all the experimentally demonstrated EP lasers at UV-B and -C, DPD was utilized within the laser epitaxial structures. The compositionally-graded AlGaN layers have their polarization charge distributed throughout the grading demonstrating high sheet carrier densities and immune to carrier freeze-out at low temperature. A hole carrier concentration of 4.2×10^{17} cm^{-3} was achieved for an undoped AlGaN layer with an average of $x = 0.86$ [154].

Figure 6a shows how compositionally graded AlGaN creates polarization-induced 3D charges that result in free carriers. The nature of the free charges, acceptors or donors is controlled by changing the direction of grading. Although hole conductivity has been achieved with DPD without doping, most *p*-type DPD studies introduced Mg doping as well despite the optical loss due to Mg-induced absorption [155–157]. To minimize Mg absorption at the DPD layer, both UV-C lasers [30,33] employed the undoped-graded AlGaN structure for DPD, while the UV-B structures introduced Mg doping to a certain degree. In the DPD structure, a two-step process with undoped AlGaN adjacent to the waveguide and *p*-doped graded AlGaN layers was implemented on the *p*-side contact of the UV-B lasers [31].
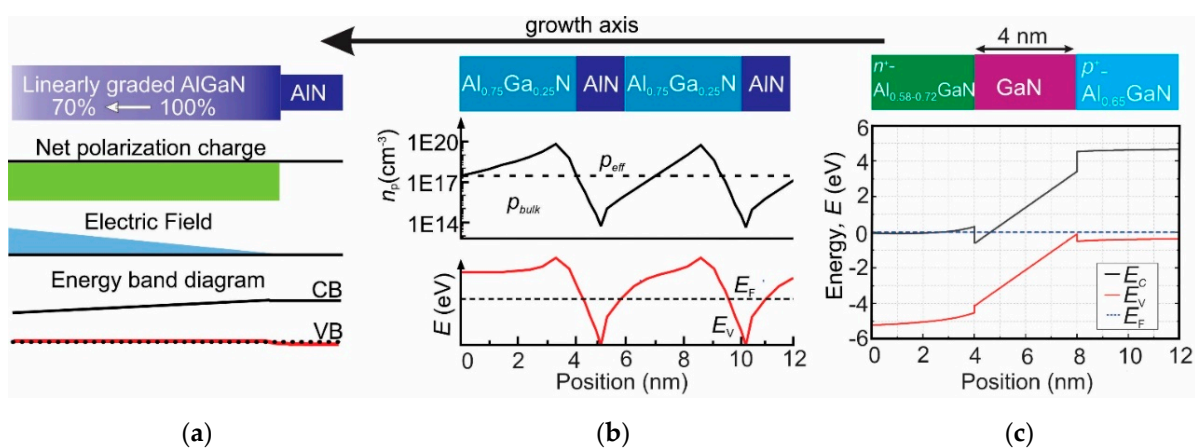

Figure 6. Schematic representation of the *p*-doping process; (**a**) schematic representation of distributed polarization doping (DPD) process for an AlGaN layer graded from $x = 0.7$ to 1, (**b**) a schematic representation of short-period superlattice (SPSL) with $Al_{0.75}Ga_{0.25}N/AlN$ alternate layers doped with 3.5×10^{19} cm^{-3} Mg generated. The dotted line represents the hole concentration for bulk $Al_{0.75}Ga_{0.25}N$ with equal doping, and (**c**) band diagram of a *p*-AlGaN/i-InGAN/*n*-AlGaN TJ.

Because of very little difference in refractive index for Al-rich AlGaN layers used in thin film based UV devices, developing proper waveguide layers has remained a major challenge. The DPD structure integration on the *p*-AlGaN side has had major success in developing the UV-lasers. Along with its intended purpose of increasing hole injection, this high Al-containing DPD layer also improves the confinement factors due to a high refractive index contrast.

4.3.2. Short-Period Superlattice

A short-period superlattice, comprising of alternate layers of $Al_xGa_{1-x}N$ with high and low x doped with Mg ($Al_xGa_{1-x}N/Al_yGa_{1-y}N$ with $x > y$) was used to improve hole activation with the help of band offset and strong built-in spontaneous and piezoelectric polarization fields instead of thermal energy [158–161]. By improving vertical conductivity, the resistance of an SPSL reduced nearly 12 times compared to a bulk layer with the same composition, making the SPSL layer suitable to operate at a high voltage [56]. A hole concentration of 3.4×10^{18} cm^{-3} and resistivity of 6.4 Ω-cm for a 200 nm-thick $Al_{0.8}Ga_{0.2}N$ layer was achieved by controlling the SL period and well thickness [160]. A schematic diagram along with band structure is shown in Figure 6b. The strong electric field built at the barrier and well enhances the ionization of Mg acceptors and reduces the activation

energy from above 400 meV to 40–67 meV for $Al_xGa_{1-x}N$ layers with $x = 0.8$. Besides hole-conductivity, the high Al-containing cladding layer [56] is also required for good optical confinement to reduce optical loss. Martens et al. experimented on different SPSL cladding layers with an average x of 0.37, 0.57 and 0.81 to investigate the optical loss and developed low-loss, highly-conductive p-AlGaN, being suitable for EP UV-C lasers [56]. The work demonstrated a positive slope in series resistance as x increases, while nearly an order of magnitude reduction in series resistance is obtained for lasers with p-SPSL compared to the devices with uniform composition [56].

4.3.3. Tunnel Junctions (TJs)

While efficient hole injection is feasible for UV lasers using DPD and SPSL structures, absorption and Joule heating at p-AlGaN leads to high internal loss and large series resistance, resulting in a high threshold. With the help of polarization doping, successful demonstration of GaN-based TJ was reported since 2001 [162] and in 2016 the first AlGaN based TJ was reported [163]. While p-AlGaN is necessary for p-side cladding, implementing a TJ eliminates the thick p-cladding layer requirement. The use of TJs as an intracavity contact for hole injection through interband tunneling is reported in a number of experimental studies [55,150,151,164,165]. With the non-equilibrium hole injection and ultra-low absorption at the TJ interface, the introduction of TJ simultaneously improves hole injection. So far, TJ has successfully been implemented only in UV-C LEDs based on both thin films [165] and NWs [166]. Hence, the TJ is another potential candidate for solving the problem of hole injection for making conductive p-AlGaN even with high x.

TJ resistance as low as 2×10^{-3} Ω-cm^2 was achieved for structures with $x = 0.7$ [165]. The resistance however increased significantly once the x is further increased due to the increase of tunnel barrier, raising the voltage penalty subsequently. To reduce the voltage penalty, the use of an ultra-thin InGaN layer in between the p^+- and n^+-AlGaN are described [163]. The insertion of a lower-bandgap InGaN, however, could dramatically increase the optical loss and subsequent threshold current increase that will very likely prevent devices from lasing. FP edge-emitting sub-300 nm lasers with "offset quantum-well" design to reduce optical loss on the p-cladding side with p^+-AlGaN/i-GaN/n^+-AlGaN TJs were recently proposed (see Figure 6c) [100,101].

4.4. Active Region

The low differential efficiency of UV-B and UV-C lasers may not be completely related to insufficient hole generation and injection mechanism, as explained in Section 4.3. For the successful design and demonstrations of UV-B and -C lasers, one primarily requires a good AlGaN-based active region to obtain high material gain [22,53,154]. This includes not only a good material quality with low-defects and sharp interfaces but also an optimal number of QWs, and the right thicknesses of QWs and barrier with optimal band offsets and adjusting the waveguide thickness [16,167,168]. These considerations will be added by the polarization switching phenomena of emitted light for the unique AlGaN material system [169,170]. Using a higher number of QWs appears to be non-conventional in the wavelengths of interest due to the constraint of uniform pumping of all the QWs with carriers to obtain material gain. If one of the quantum wells cannot be pumped enough, they will operate as a band-edge absorbing layer and then it fails to lase.

As far as the UV-A regime goes, a different trend holds. References [18,60], reporting UV-A emission, used three 3 nm thick QWs [171]. As opposed to conventional III-nitride laser structures, EP UV-B and -C lasers used relatively thicker QWs in active regions. One is often interested in a modal gain which is material gain times transverse confinement factor. Therefore, a thicker QW provides higher modal gain, however, at the expense of poor overlap between electron and hole wave functions in III-nitrides. Zhang et al. [30] in their first EP UV-C laser used a 9 nm thick compositionally-optimized AlGaN layer to emit at 271.8 nm [30]. This provided a transverse confinement factor of 2.9%. Compared to UV-C lasers, UV-B lasers used a slightly lower Al composition, i.e., $x = 0.35$ in the active

region [31] with SQW of similar thickness or MQW of lower thickness. While all previously reported structures [30,31,33] used identical thickness, a double QW-based active region with a well thickness of 4 nm and barrier 8 nm was used to demonstrate nearly 40% improvement in threshold current with no change in emission wavelength [32].

Contrary to thin multi-QW based active regions used in conventional diode lasers, NW laser structures implemented "thick layer-based" unique active regions [27–29]. Interestingly, it was found that Al-rich AlGaN NWs feature extensive Ga-rich nanoclusters. The atomic scale Ga-rich AlGaN striation laterally exhibit discontinuity in the direction perpendicular to NW growth [27]. This indicates that atomic-scale compositional fluctuations possess quantum dot/dash-like structural characteristics within the Al-rich NWs. Such Ga-rich *i*-AlGaN nanoclusters have thicknesses varying from 0.25–2 nm along the growth direction, and lateral sizes in the range of 2–10 nm. Hence, the spontaneously formed quantum dot/dashes embedded within the *i*-AlGaN layer serves as an active region, providing strong 3D confinement and high material gain.

5. Demonstration of AlGaN Lasers

Significant efforts have already been undertaken to develop EP UV-B and -C lasers using thin film based epi-structures. With the recent advancement in high-quality AlN bulk- or AlN/sapphire templated substrates, low-defect active epilayers and improved hole injection, EP AlGaN lasers have turned into reality. To the best of our knowledge, only two research teams worldwide have recently experimentally demonstrated EP AlGaN lasers which will now be discussed. The structural descriptions and the achieved results of each device will also be briefly provided. The discussion is classified based on the material types used in the devices.

5.1. Thin Film Lasers

In 2019, the first thin film-based EP AlGaN laser at UV-C was achieved by researchers at Nagoya University, Japan, in cooperation with Asahi Kasei Corporation, Chiyoda City, Japan and Crystal IS, Inc., Green Island, NY, USA [30]. The laser materials were pseudomorphically grown on (0001) bulk AlN substrates by MOCVD. The devices used a single AlGaN 9-nm-thick QW to emit at 271.8 nm. For hole injection, pseudomorphic DPD layers were used on top of *p*-waveguide. Figure 7a schematically shows the fully processed FP lasers.
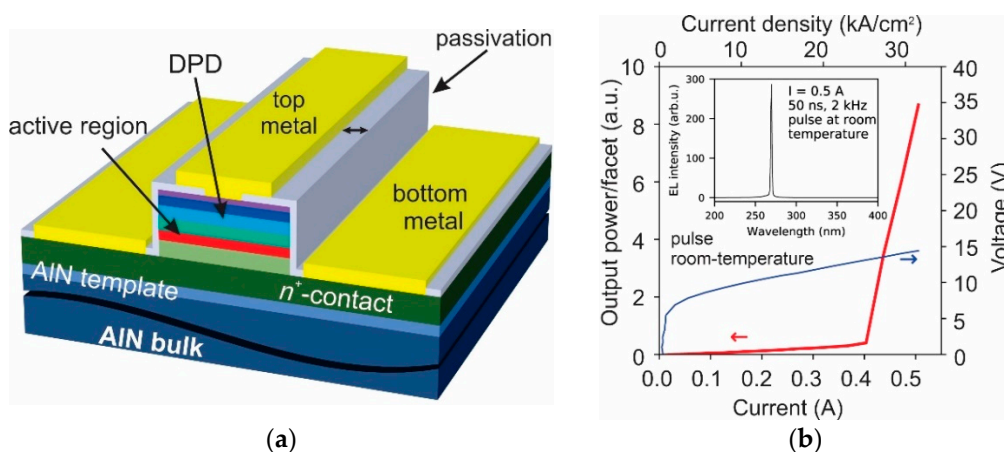

Figure 7. (**a**) Schematic cross-section of fully-processed UV-C laser and (**b**) its *L-I-V* characteristics. (**b**) is reproduced with permission from reference [30]. Copyright (2019) The Japan Society of Applied Physics.

The light-current-voltage (*L-I-V*) characteristics of the devices are shown in Figure 7b. The devices operated at RT under pulse conditions. The measured threshold voltage and current density of the devices were 13.8 V and 25 kA/cm^2, respectively. The spectral characteristics of the devices are shown in the inset of Figure 7b. Despite the low oper-

ating voltage (voltage drop across the active region ~4.6 V), the large threshold current density observed hindered the CW operation of such devices. The lasers operated only under extremely short current-pulses of 50 ns and a repetition frequency of 2 kHz. This breakthrough was ascribed to a low defect density AlN substrate and incorporation of a polarization doped Mg-free *p*-AlGaN DPD-based cladding layer.

The same research team engineered the same laser epilayers by combining dry and wet etching [172–174] to form smooth-vertical sidewalls on mirror facets [33]. The facets were then coated with a distributed Bragg reflector (DBR) composed of HfO_2 and Al_2O_3, yielded 49.6% reflectivity. This significantly reduced the threshold current density of the device [175]. A cross-sectional scanning electron microscopy image with DBR coating is shown in Figure 8a. The *L-I-V* characteristics are shown in Figure 8b with the lasing spectrum in the inset. Despite the same epilayers in reference [30], the devices emitted at a peak reflectivity of DBR, i.e., 278.9 nm. The measured threshold current density of the device was 19.6 kA/cm^2. The authors demonstrated the process steps used in fabricating these devices over a 2″ wafer, showing a promise of large-area production in the future.
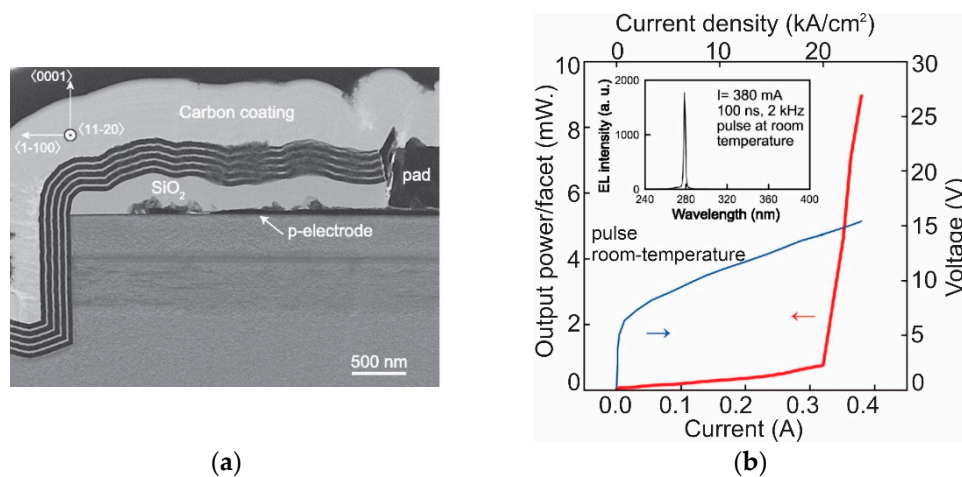

(**a**)   (**b**)

Figure 8. (**a**) Scanning electron microscopy (SEM) cross-section of UV-C laser with vertical sidewalls and distributed Bragg reflector (DBR) coating, and (**b**) and its *L-I-V* characteristics. The lasing spectrum is shown in the inset. Figures are reproduced with permission from Reference [33]. Copyright (2020) AIP Publishing LLC.

In the next year, the achievement of demonstrating the first UV-B diode laser was reported by the industry researchers from Asahi Kasei Corporation, Chiyoda City, Japan, in collaboration with Meijo University, Mie University and Nagoya University, Japan [31]. Unlike the UV-C devices, the UV-B devices used the epilayers grown on top of AlN/sapphire templates. The laser structures remain nearly the same as reference [30] except for the use of $Al_{0.35}Ga_{0.65}$N-QW as a gain medium.

Figure 9a presents the *L-I-V* characteristics for the UV-B lasers. The threshold current density and voltage were 41 kA/cm^2 and 27 V, respectively, which were much higher than the UV-C lasers [30,33]. A much higher threshold voltage was attributed to a large voltage drop at *n*- and *p*-contacts of the devices. The threshold current was experimentally confirmed to be highly sensitive to the *p*-contact width of the devices. To be specific, more than 400% reduction in threshold current was obtained by increasing the contact width from 2 μm to 11.5 μm. Figure 9b presents the current-dependent spectra, showing multimode emission around 298 nm.

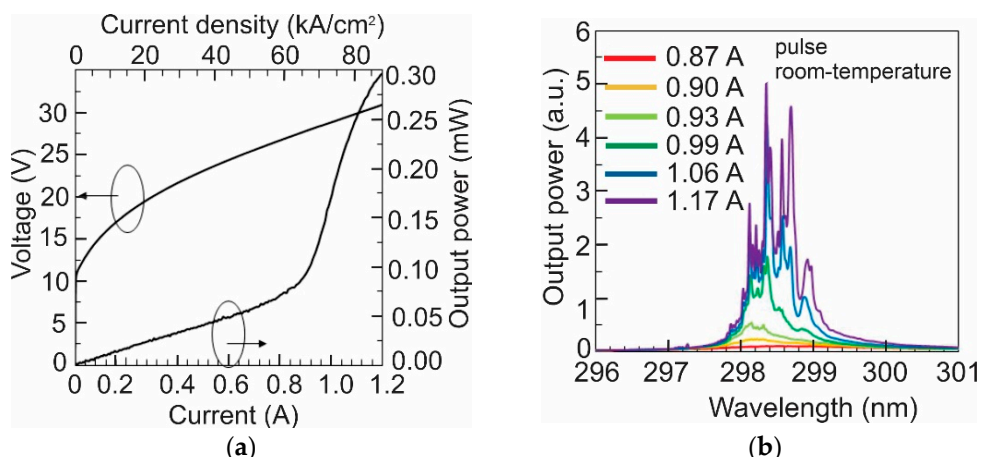**Figure 9.** (**a**) L-I-V characteristics for the UV-B lasers, and (**b**) emission spectra of the laser at different current bias. Figures are reproduced with permission from reference [31]. Copyright (2020) The Japan Society of Applied Physics.

A few months after the previous demonstration, Omori et al. from the same group reported another UV-B lasers emitting at 298 nm [32]. Compared to the previous structure, this laser structure used a two QW-based design and a thicker waveguide layer, yielding a larger modal gain due to a higher confinement factor. Figure 10a presents *L-J-V* characteristics with different cavity length. The pulsed threshold current density was 25 kA/cm^2. In addition to the highly-resistive *n*- and *p*-contacts, high absorption loss at the highly graded *p*-layer was attributed to the high threshold current. The high threshold voltage also forced to operate this device under pulse conditions. It was experimentally verified that the AlN molar grading at the DPD cladding layer had no significant influence on the internal loss owing to the polarization doping instead of impurity doping. Hence, the device epilayer design was considered as a suitable optical resonator after determining the internal loss to a few cm^{-1}. Very recently, a follow-up experimental study, investigating the carrier injection efficiency in the same laser structure, has been conducted by Sato et al. [37]. An imbalance in carrier injection leading to electron overflow was found responsible for the high threshold current density for the UV-B lasers and can be overcome by improving injection efficiency and obtaining highly-reflective mirror facets.
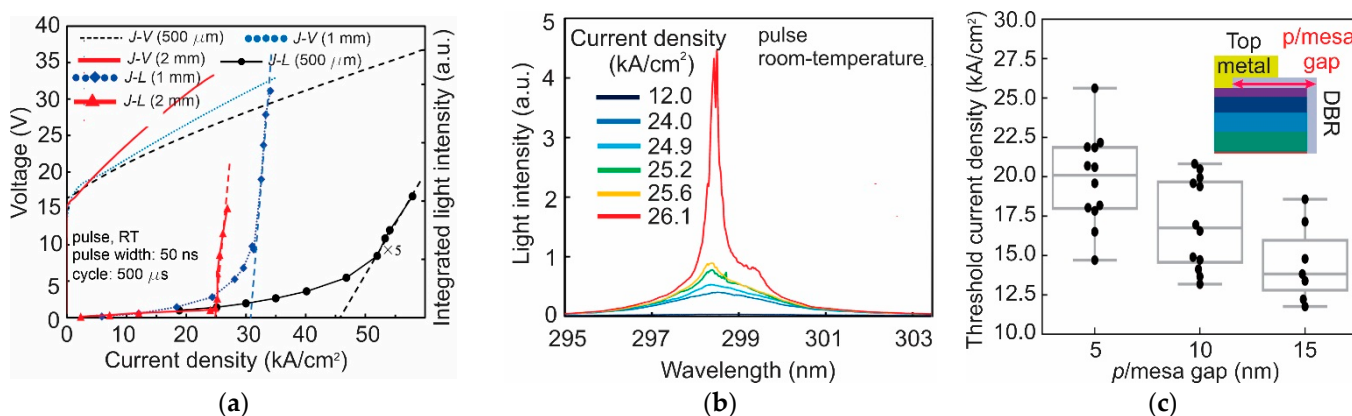

Figure 10. (**a**) *L-J-V* characteristics, (**b**) electrical current density dependent emission spectra of the UV-B lasers, and (**c**) threshold current density with respect to different p/mesa gap widths. (**a**,**b**) are reproduced with permission from reference [32]. Copyright (2020) The Japan Society of Applied Physics (**c**) is reproduced with permission from Reference [34]. Copyright (2021) The Japan Society of Applied Physics.

To further investigate the high threshold current for UV-lasers and possible ways to reduce it, very recently Kushimoto et al. reported the impact of the heat treatment on

lasers [34]. Experiments revealed that the dark spots at the active region near the mesa sidewalls appeared after heat treatment and were directly related to point defects created during dry etch. The point defects diffused from the sidewalls to the device gain medium, introducing non-uniformity in active area composition [176,177]. To avoid these dark spots, depositing the *p*-contact away from the sidewall was experimentally confirmed to be better. The threshold current density as a function of the p/mesa gap is presented in Figure 10c. The wider mesa area allowed metal contacts to keep a higher gap from the sidewalls. Hence, a reduction in threshold current density was observed with increasing the *p*/mesa gap.

As an extension of the early UV-B laser effort of reference [32] for further improvement in device performance, the same set of Japanese academic and industry researchers very recently published new results. Using the same epi-layer structure of reference [32], the role of waveguide layer and *p*-type cladding layer thickness on the threshold current density of a device [35] was carefully analyzed. By reducing waveguide layer thickness from 150 nm to 50 nm and changing the *p*-type waveguide composition as well as doping, UV-B lasers emitting 300 nm with a threshold current density of 13.3 kA/cm^2 were achieved. Figure 11a,b represents the *L-J-V* characteristics for the improved lases along with the laser diode reported in reference [32] and the emission spectra, respectively. The *p*-type doping optimization placed a significant effect on the reduction of the turn-on voltage and differential resistance. The waveguide layer thickness reduction on the other hand improved the injection efficiency and optical confinement factor resulting in the record-low threshold current density at the UV-B spectral band.
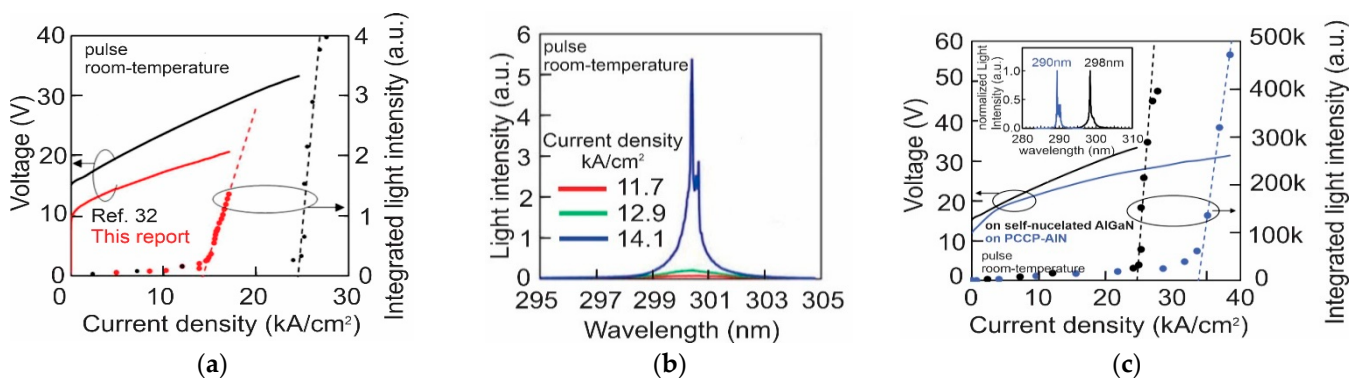

Figure 11. *L-J-V* characteristics of the UV-B laser with *p*-electrode width of 10 μm plotted along with the UV-B laser reported in reference [32], (**b**) emission spectra of the laser with *p*-electrode width of 15 μm at different current bias, (**c**) *L-J-V* characteristics of the UV-B laser grown on different AlGaN template. The lasing spectra are shown in the inset. (**a**,**b**) are reproduced with permission from reference [35]. (**c**) is reproduced with permission from Reference [36]. Copyright (2021) The Japan Society of Applied Physics.

At nearly the same time as their earlier publication [35], the same researcher also demonstrated a UV-B laser grown on the novel patterned AlN template (see Figure 5e) [36]. The objective behind employing a patterned AlN template was to achieve a controlled 3D growth of AlGaN film to reduce dislocation formation. Compared to the epi-layer structure [32] grown on a self-nucleated AlN sample, the PCCP-ALN-based lasers showed 10 kA/cm^2 higher threshold current density as well as 8 nm red shift in the lasing wavelength as shown in Figure 11c. The higher threshold current density observed in the study was mainly attributed to higher defect density in AlGaN films on PCCP-AlN templates.

5.2. Nanowire Lasers

While the thin film-based UV-optoelectronics was battling against high-quality substrates along with *p*-doping, nearly defect-free AlGaN NWs is possible on Si using MBE [42,44,178]. Spontaneously grown NWs show excellent lateral and transverse optical confinement and

bring inherent advantage of the ease of *p*-dopant incorporation. Since the first demonstration in 2015, the evolution of NW-based EP UV-B and -C lasers will now be reviewed.

Three experimental demonstrations of NW-based EP AlGaN lasers in the wavelengths of interest are reported so far [27–29]. All of these three reports were made by the same research group from McGill University, Canada. The type of cavity adopted in all these studies used random NW arrays, yielding random lasing [179,180]. Figure 12a shows the schematic of AlGaN NW array lasers. The NW structure consisted of GaN:Si ($\sim$250 nm), AlGaN:Si ($\sim$100 nm), AlGaN ($\sim$100 nm), AlGaN:Mg ($\sim$100 nm), and GaN:Mg ($\sim$10 nm) segments. The devices were designed to act as surface-emitting lasers although there was $\sim$20 nm-thick metal *p*-contact on the top with negligible absorption.
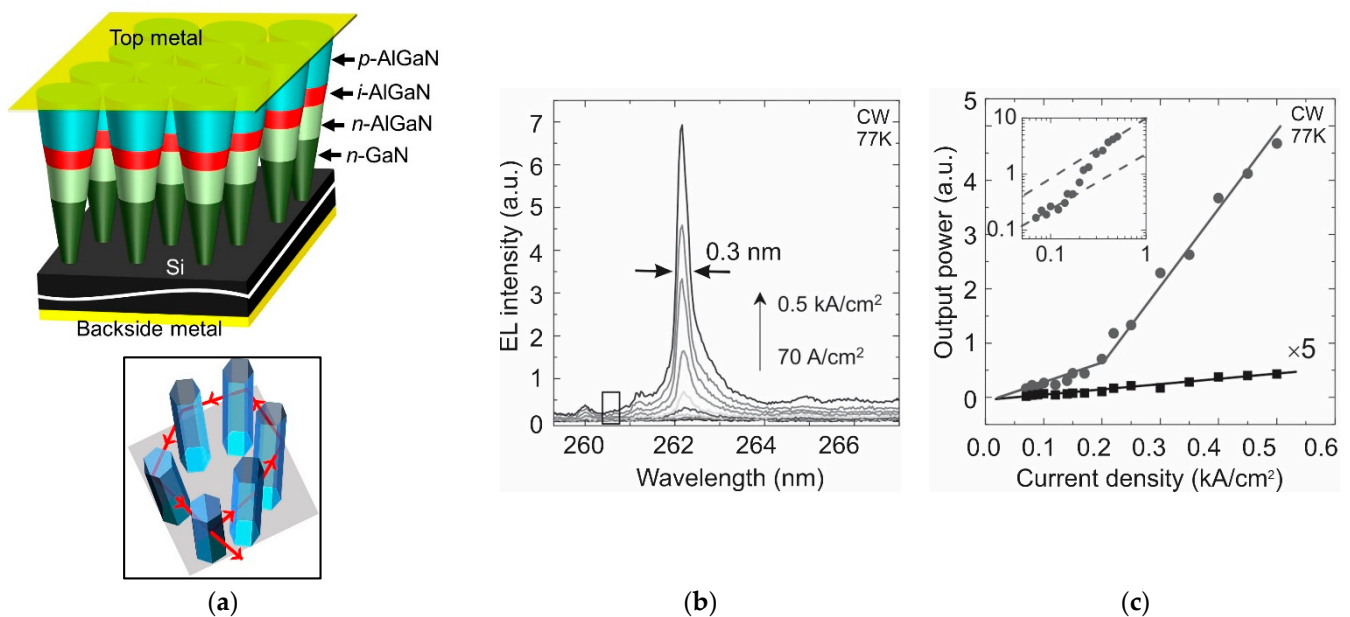

(a)   **(b)**   **(c)**

Figure 12. (**a**) Three-dimensional schematic representation of the fully-processed random lasers. Inset shows the mechanism for random laser emission, (**b**) electroluminescence (EL) emission spectra measured under different current densities, and (**c**) integrated EL intensity as a function of the injection current for the NW laser. Figures are reproduced with permission from Reference [28]. Copyright (2015) AIP Publishing LLC.

In 2015, the first development was related to CW-operating EP lasers emitting at 262.1 nm [28]. The fully-processed device schematic is shown in Figure 12a. The first-ever EP UV-C lasers also reported the lowest threshold current density till date. The EL characteristics is shown in Figure 12b. The extracted *L-I* characteristics of the random lasers is presented in Figure 12c. The inset shows the *L-I* curve of the 289 nm lasing peak in a logarithmic scale. A low threshold current density of 0.2 kA/cm^2 for a lasing area of 10 μm^2 was observed for the devices. However, the device operation was limited to a cryogenic temperature, i.e., 77 K [28]. The inability to operate at RT was attributed to reduced gain due to the very large inhomogeneous broadening of quantum dots embedded in NWs and unoptimized cavity design.

Again a few months later, UV-B lasing from single-crystalline AlGaN NWs was demonstrated by the same research team from McGill University [27]. Figure 13a shows the current dependent EL spectra with a peak at 289 nm. The extracted *L-I* characteristics of the random lasers are presented in Figure 13b. Owing to the optimized 3D optical confinement structure, the threshold current density reduced to 0.3 kA/cm^2 under CW operation. The lasing area was 10 μm^2.
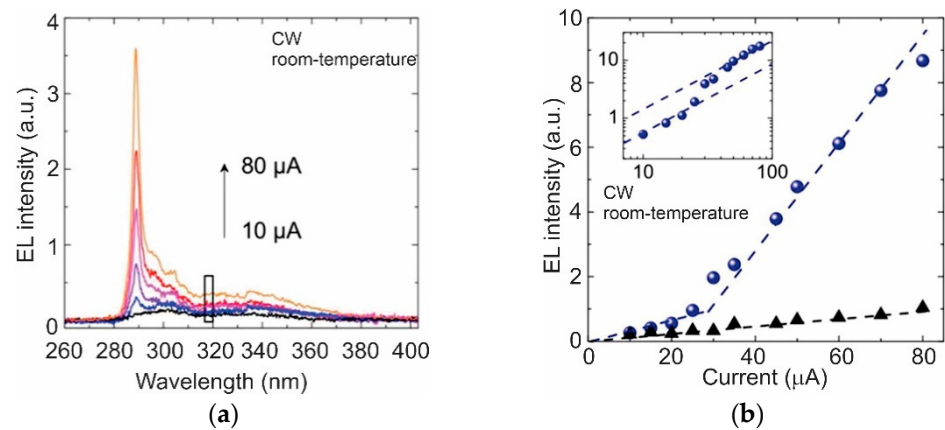
Figure 13. UV-C lasing characteristics at RT, (**a**) EL emission spectra measured under different current densities, and (**b**) integrated EL intensity as a function of the injection current. Figures are reproduced with permission from reference [27]. Copyright (2015) AIP Publishing LLC.

Despite the advantage of obtaining strong optical confinement, the quantum dot generation due to compositional variation at the *i*-AlGaN active region limits the shortest achievable lasing wavelength [28,181]. In 2016, the same research group for the third time addressed this issue and successfully achieved record short 239 nm lasing emission with improved uniformity and higher Al incorporation in the laser devices [29]. The tapered structure and the epilayers' design and the resonator type all were kept unchanged except slight reduction in *i*-AlGaN thickness. Figure 14a shows the applied current-dependent EL spectra with much shorter linewidth compared to the previously reported results. RT and CW operation was observed from the devices. This is the shortest wavelength reported to date for any EP AlGaN laser. Figure 14b shows the extracted *L-I* characteristics for the random lasers at 239 nm.
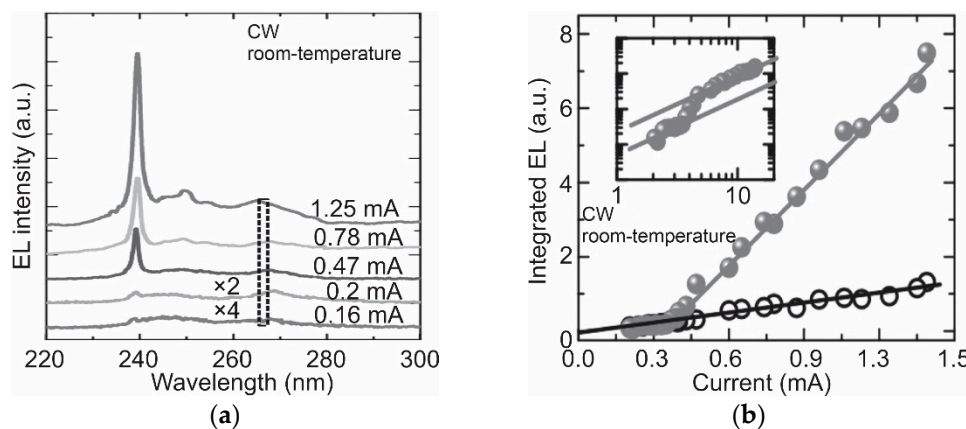

Figure 14. UV-B lasing characteristics at room temperature (RT) (**a**) the EL emission spectra measured under different current density, and (**b**) integrated EL intensity as a function of the injection current density. Figures are reproduced with permission from reference [29]. Copyright (2016) AIP Publishing LLC.

6. Conclusions

The ultrawide bandgap AlGaN materials system offers the greatest promise for realizing compact and efficient diode lasers in the UV-B and -C spectral bands. This review provides the current status and issues in the development of EP AlGaN-based UV-B and -C diode lasers which serve as a critical component of future photonic devices and subsystems. Materials challenges are discussed in detail in four critical technical areas that require close attention for the successful implementation of emitters at these spectral bands. Compared to UV-B lasers, the reported UV-C lasers showed relatively better device performance due

to the use of low-defect density bulk AlN substrates. Finding the right substrate materials for UV-B is not trivial. AlGaN templates with a target Al composition on AlN substrates have not yet shown their full potential in terms of working devices. Only sapphire template substrates with controlled strain engineering generated the working UV-B lasers so far.

Although EP thin film-based UV-B and UV-C lasers have been reported only very recently, they operated at a very high threshold current density and only under pulsed conditions. Compared to better-performing UV-A lasers, the devices under interest exhibited threshold current density ×3–4 higher. Hence, reducing threshold current density for UV-B and UV-C lasers to <10 kAcm^{-2} is important to achieve CW operation. High optical losses and poor injection efficiency are the two potential issues of high threshold current density, which should be improved. An optimized heterostructure design, good active region by preventing electron overflow over QWs, balanced carrier injection, excellent thermal management and high-quality AlGaN layers are essential to obtain a reasonable optical loss and injection efficiency, enabling CW- and room temperature operating lasers with a low-threshold current.

All the reported EP AlGaN NW UV-B and -C lasers used a random cavity, where the resonance cannot be controlled precisely. For real-world applications, a controlled cavity with a defined resonance is necessary. Using AlGaN NWs grown on patterned substrates and exploiting photonic crystal effects could be a few possible solutions towards making application-suited devices. In addition to patterned growth, controlling NW geometry and spacing amongst the NWs, material bandgap engineering, excellent sidewall smoothness and surface quality are also important for the development of high-efficiency AlGaN NW-based UV-B and -C lasers.

The device physics of UV-B and -C lasers is still under investigation and a significant amount of work still has to be done to improve the laser performances. The state-of-the-art laser results consolidated in this review suggest the feasibility of EP lasing from AlGaN-based thin-film and NW material platforms. Further development of metal contacts especially on the *p*-side, *p*-SPSL cladding layer or low-resistive AlGaN TJ for improved hole injection are required in order to reach high carrier densities and obtain lasing. All in all, with the progress that has already been made and the potential solutions for some of the technical challenges, together with the technological advancement, this highly-demanding laser technology is expected to see rapid development over time. Continued and extended efforts will pave the way to achieve application-suitable lasers at these spectral bands and more critical breakthroughs are anticipated within the next few years.

Author Contributions: Conceptualization, S.M.N.H., W.Y. and S.A.; writing—review and editing, S.M.N.H., W.Y., M.S.I.S. and S.A. All authors have read and agreed to the published version of the manuscript.

Conflicts of Interest: The authors declare no conflict of interest.

References

1. Majumdar, A.K. Non-line-of-sight (NLOS) ultraviolet and indoor free-space optical (FSO) communications. In *Advanced Free Space Optics (FSO)*; Springer: Berlin/Heidelberg, Germany, 2015; pp. 177–202.
2. Reilly, D.M.; Moriarty, D.T.; Maynard, J.A. Unique properties of solar blind ultraviolet communication systems for unattended ground sensor networks. In Proceedings of the Unmanned/Unattended Sensors and Sensor Networks, London, UK, 1 September 2004; pp. 244–254.
3. Bhar, G.; Chatterjee, U. Development of ultraviolet laser for disinfection of potable water. *Indian J. Phys.* **2006**, *80*, 517–521.
4. Vilhunen, S.; Särkkä, H.; Sillanpää, M. Ultraviolet light-emitting diodes in water disinfection. *Environ. Sci. Pollut. Res.* **2009**, *16*, 439–442. [CrossRef]
5. Grishkanich, A.; Zhevlakov, A.; Kascheev, S.; Polyakov, V.; Sidorov, I.; Ruzankina, J.; Yakovlev, A.; Mak, A. Study methods for disinfection water for injection. In Proceedings of the Biophotonics: Photonic Solutions for Better Health Care V, Brussels, Belgium, 4–7 April 2016; p. 98873K.
6. Nelson, J.S.; Berns, M.W. Laser applications in biomedicine. Part II: Clinical applications. *J. Laser Appl.* **1989**, *1*, 9–20. [CrossRef]

7.   Letokhov, V.S. Laser light in biomedicine and the life sciences: From the present to the future. In *Biomedical Photonics Handbook*; CRC Press: Boca Raton, FL, USA, 2003; pp. 177–192.

8.   Raeiszadeh, M.; Adeli, B. A Critical Review on Ultraviolet Disinfection Systems against COVID-19 Outbreak: Applicability, Validation, and Safety Considerations. *ACS Photon.* **2020**, *7*, 2941–2951. [CrossRef]

9.   Gerchman, Y.; Mamane, H.; Friedman, N.; Mandelboim, M. UV-LED disinfection of Coronavirus: Wavelength effect. *J. Photochem. Photobiol. B Biol.* **2020**, *212*, 112044. [CrossRef]

10. Armstrong, A.; Allerman, A.A.; Fischer, A.J.; King, M.P.; Van Heukelom, M.; Moseley, M.W.; Kaplar, R.; Wierer, J.; Crawford, M.H.; Dickerson, J.R. *Ultra-Wide Bandgap AlGaN Materials for Electronics and Opto-Electronics*; Sandia National Lab. (SNL-NM): Albuquerque, NM, USA, 2016.

11. Taniyasu, Y.; Kasu, M.; Makimoto, T. An aluminium nitride light-emitting diode with a wavelength of 210 nanometres. *Nature* **2006**, *441*, 325–328. [CrossRef]

12. Wagner, R.; Levitt, A.P. *Whisker Technology*; Levitt, A.P., Ed.; Wiley: New York, NY, USA, 1970; pp. 47–119.

13. Akasaki, I.; Sota, S.; Sakai, H.; Tanaka, T.; Koike, M.; Amano, H. Shortest wavelength semiconductor laser diode. *Electron. Lett.* **1996**, *32*, 1105–1106. [CrossRef]

14. Iida, K.; Kawashima, T.; Miyazaki, A.; Kasugai, H.; Mishima, S.; Honshio, A.; Miyake, Y.; Iwaya, M.; Kamiyama, S.; Amano, H. 350.9 nm UV laser diode grown on low-dislocation-density AlGaN. *Jpn. J. Appl. Phys.* **2004**, *43*, L499. [CrossRef]

15. Masui, S.; Matsuyama, Y.; Yanamoto, T.; Kozaki, T.; Nagahama, S.-I.; Mukai, T. 365 nm ultraviolet laser diodes composed of quaternary AlInGaN alloy. *Jpn. J. Appl. Phys.* **2003**, *42*, L1318. [CrossRef]

16. Kneissl, M.; Treat, D.W.; Teepe, M.; Miyashita, N.; Johnson, N.M. Ultraviolet AlGaN multiple-quantum-well laser diodes. *Appl. Phys. Lett.* **2003**, *82*, 4441–4443. [CrossRef]

17. Kneissl, M.; Yang, Z.; Teepe, M.; Knollenberg, C.; Schmidt, O.; Kiesel, P.; Johnson, N.M.; Schujman, S.; Schowalter, L.J. Ultraviolet semiconductor laser diodes on bulk AlN. *J. Appl. Phys.* **2007**, *101*, 123103. [CrossRef]

18. Yoshida, H.; Yamashita, Y.; Kuwabara, M.; Kan, H. A 342-nm ultraviolet AlGaN multiple-quantum-well laser diode. *Nat. Photon.* **2008**, *2*, 551–554. [CrossRef]

19. Aoki, Y.; Kuwabara, M.; Yamashita, Y.; Takagi, Y.; Sugiyama, A.; Yoshida, H. A 350-nm-band GaN/AlGaN multiple-quantum-well laser diode on bulk GaN. *Appl. Phys. Lett.* **2015**, *107*, 151103. [CrossRef]

20. Wunderer, T.; Chua, C.; Northrup, J.; Yang, Z.; Johnson, N.; Kneissl, M.; Garrett, G.; Shen, H.; Wraback, M.; Moody, B. Optically pumped UV lasers grown on bulk AlN substrates. *Phys. Status Solidi C* **2012**, *9*, 822–825. [CrossRef]

21. Kirste, R.; Guo, Q.; Dycus, J.H.; Franke, A.; Mita, S.; Sarkar, B.; Reddy, P.; LeBeau, J.M.; Collazo, R.; Sitar, Z. 6 kW/cm2 UVC laser threshold in optically pumped lasers achieved by controlling point defect formation. *Appl. Phys. Express* **2018**, *11*, 082101. [CrossRef]

22. Guo, Q.; Kirste, R.; Reddy, P.; Mecouch, W.; Guan, Y.; Mita, S.; Washiyama, S.; Tweedie, J.; Sitar, Z.; Collazo, R. Impact of the effective refractive index in AlGaN-based mid-UV laser structures on waveguiding. *Jpn. J. Appl. Phys.* **2020**, *59*, 091001. [CrossRef]

23. Kawase, Y.; Ikeda, S.; Sakuragi, Y.; Yasue, S.; Iwayama, S.; Iwaya, M.; Takeuchi, T.; Kamiyama, S.; Akasaki, I.; Miyake, H. Ultraviolet-B band lasers fabricated on highly relaxed thick Al0. 55Ga0. 45N films grown on various types of AlN wafers. *Jpn. J. Appl. Phys.* **2019**, *58*, SC1052. [CrossRef]

24. Kuhn, C.; Martens, M.; Mehnke, F.; Enslin, J.; Schneider, P.; Reich, C.; Krueger, F.; Rass, J.; Park, J.B.; Kueller, V. Influence of waveguide strain and surface morphology on AlGaN-based deep UV laser characteristics. *J. Phys. D Appl. Phys.* **2018**, *51*, 415101. [CrossRef]

25. Zhao, S.; Connie, A.; Dastjerdi, M.; Kong, X.; Wang, Q.; Djavid, M.; Sadaf, S.; Liu, X.; Shih, I.; Guo, H. Aluminum nitride nanowire light emitting diodes: Breaking the fundamental bottleneck of deep ultraviolet light sources. *Sci. Rep.* **2015**, *5*, 8332. [CrossRef]

26. Li, K.; Liu, X.; Wang, Q.; Zhao, S.; Mi, Z. Ultralow-threshold electrically injected AlGaN nanowire ultraviolet lasers on Si operating at low temperature. *Nat. Nanotechnol.* **2015**, *10*, 140. [CrossRef]

27. Zhao, S.; Woo, S.; Bugnet, M.; Liu, X.; Kang, J.; Botton, G.; Mi, Z. Three-dimensional quantum confinement of charge carriers in self-organized AlGaN nanowires: A viable route to electrically injected deep ultraviolet lasers. *Nano Lett.* **2015**, *15*, 7801–7807. [CrossRef] [PubMed]

28. Zhao, S.; Liu, X.; Woo, S.; Kang, J.; Botton, G.; Mi, Z. An electrically injected AlGaN nanowire laser operating in the ultraviolet-C band. *Appl. Phys. Lett.* **2015**, *107*, 043101. [CrossRef]

29. Zhao, S.; Liu, X.; Wu, Y.; Mi, Z. An electrically pumped 239 nm AlGaN nanowire laser operating at room temperature. *Appl. Phys. Lett.* **2016**, *109*, 191106. [CrossRef]

30. Zhang, Z.; Kushimoto, M.; Sakai, T.; Sugiyama, N.; Schowalter, L.J.; Sasaoka, C.; Amano, H. A 271.8 nm deep-ultraviolet laser diode for room temperature operation. *Appl. Phys. Express* **2019**, *12*, 124003. [CrossRef]

31. Sato, K.; Yasue, S.; Yamada, K.; Tanaka, S.; Omori, T.; Ishizuka, S.; Teramura, S.; Ogino, Y.; Iwayama, S.; Miyake, H. Room-temperature operation of AlGaN ultraviolet-B laser diode at 298 nm on lattice-relaxed Al0. 6Ga0. 4N/AlN/sapphire. *Appl. Phys. Express* **2020**, *13*, 031004. [CrossRef]

32. Omori, T.; Ishizuka, S.; Tanaka, S.; Yasue, S.; Sato, K.; Ogino, Y.; Teramura, S.; Yamada, K.; Iwayama, S.; Miyake, H. Internal loss of AlGaN-based ultraviolet-B band laser diodes with p-type AlGaN cladding layer using polarization doping. *Appl. Phys. Express* **2020**, *13*, 071008. [CrossRef]

33. Sakai, T.; Kushimoto, M.; Zhang, Z.; Sugiyama, N.; Schowalter, L.J.; Honda, Y.; Sasaoka, C.; Amano, H. On-wafer fabrication of etched-mirror UV-C laser diodes with the ALD-deposited DBR. *Appl. Phys. Lett.* **2020**, *116*, 122101. [CrossRef]

34. Kushimoto, M.; Zhang, Z.; Sugiyama, N.; HONDA, Y.; Schowalter, L.J.; Sasaoka, C.; Amano, H. Impact of heat treatment process on threshold current density in AlGaN-based deep-ultraviolet laser diodes on AlN substrate. *Appl. Phys. Express* **2021**, *14*, 051003. [CrossRef]

35. Tanaka, S.; Ogino, Y.; Yamada, K.; Omori, T.; Ogura, R.; Teramura, S.; Shimokawa, M.; Ishizuka, S.; Yabutani, A.; Iwayama, S. AlGaN-based UV-B laser diode with a high optical confinement factor. *Appl. Phys. Lett.* **2021**, *118*, 163504. [CrossRef]

36. Tanaka, S.; Teramura, S.; Shimokawa, M.; Yamada, K.; Omori, T.; Iwayama, S.; Sato, K.; Miyake, H.; Iwaya, M.; Takeuchi, T. AlGaN-based UV-B laser diode with a wavelength of 290 nm on 1 µm periodic concavo–convex pattern AlN on a sapphire substrate. *Appl. Phys. Express* **2021**, *14*, 055505. [CrossRef]

37. Sato, K.; Omori, T.; Yamada, K.; Tanaka, S.; Ishizuka, S.; Teramura, S.; Iwayama, S.; Iwaya, M.; Miyake, H.; Takeuchi, T. Analysis of carrier injection efficiency of AlGaN UV-B laser diodes based on the relationship between threshold current density and cavity length. *Jpn. J. Appl. Phys.* **2021**, *60*, 074002. [CrossRef]

38. Knelangen, M.; Consonni, V.; Trampert, A.; Riechert, H. In situ analysis of strain relaxation during catalyst-free nucleation and growth of GaN nanowires. *Nanotechnology* **2010**, *21*, 245705. [CrossRef] [PubMed]

39. Chen, Y.; Washburn, J. Structural transition in large-lattice-mismatch heteroepitaxy. *Phys. Rev. Lett.* **1996**, *77*, 4046. [CrossRef] [PubMed]

40. Fang, Z.; Robin, E.; Rozas-Jiménez, E.; Cros, A.; Donatini, F.; Mollard, N.; Pernot, J.; Daudin, B. Si donor incorporation in GaN nanowires. *Nano Lett.* **2015**, *15*, 6794–6801. [CrossRef] [PubMed]

41. Xie, P.; Hu, Y.; Fang, Y.; Huang, J.; Lieber, C.M. Diameter-dependent dopant location in silicon and germanium nanowires. *Proc. Natl. Acad. Sci. USA* **2009**, *106*, 15254–15258. [CrossRef] [PubMed]

42. Mi, Z.; Zhao, S.; Woo, S.; Bugnet, M.; Djavid, M.; Liu, X.; Kang, J.; Kong, X.; Ji, W.; Guo, H. Molecular beam epitaxial growth and characterization of Al (Ga) N nanowire deep ultraviolet light emitting diodes and lasers. *J. Phys. D Appl. Phys.* **2016**, *49*, 364006. [CrossRef]

43. Nagasawa, Y.; Hirano, A. A review of AlGaN-based deep-ultraviolet light-emitting diodes on sapphire. *Appl. Sci.* **2018**, *8*, 1264. [CrossRef]

44. Zhao, S.; Lu, J.; Hai, X.; Yin, X. AlGaN nanowires for ultraviolet light-emitting: Recent progress, challenges, and prospects. *Micromachines* **2020**, *11*, 125. [CrossRef]

45. Zhao, S.; Mi, Z. *AlGaN Nanowires: Path to Electrically Injected Semiconductor Deep Ultraviolet Lasers*; IEEE: Piscataway, NJ, USA, 2018; Volume 54, pp. 1–9.

46. Wernicke, T.; Sulmoni, L.; Kuhn, C.; Tränkle, G.; Weyers, M.; Kneissl, M. Group III-Nitride-Based UV Laser Diodes. In *Semiconductor Nanophotonics: Materials, Models, and Devices*; Kneissl, M., Knorr, A., Reitzenstein, S., Hoffmann, A., Eds.; Springer International Publishing: Cham, Switzerland, 2020; pp. 505–548.

47. Wunderer, T.; Northrup, J.E.; Johnson, N.M. AlGaN-based ultraviolet laser diodes. *III-Nitride Ultrav. Emit.* **2016**, 193–217.

48. Li, D.; Jiang, K.; Sun, X.; Guo, C. AlGaN photonics: Recent advances in materials and ultraviolet devices. *Adv. Opt. Photon.* **2018**, *10*, 43–110. [CrossRef]

49. Arafin, S.; Liu, X.; Mi, Z. Review of recent progress of III-nitride nanowire lasers. *J. Nanophoton.* **2013**, *7*, 074599. [CrossRef]

50. Zhang, Q.; Yin, X.; Zhao, S. Recent Progress on Aluminum Gallium Nitride Deep Ultraviolet Lasers by Molecular Beam Epitaxy. *Phys. Status Solidi (RRL)–Rapid Res. Lett.* **2021**, 2100090. [CrossRef]

51. Electronics, B. UV Light Emitting DIodes (UV A/B/C LEDs). Available online: https://www.boselec.com/product-category/uv-light-emitting-diodes-uv-led (accessed on 7 July 2021).

52. Lumileds. LUXEON UV LEDs. Available online: https://www.lumileds.com/products/uv-leds/ (accessed on 7 July 2021).

53. Zhang, Z.; Kushimoto, M.; Sakai, T.; Sugiyama, N.; Schowalter, L.J.; Sasaoka, C.; Amano, H. Design and characterization of a low-optical-loss UV-C laser diode. *Jpn. J. Appl. Phys.* **2020**, *59*, 094001. [CrossRef]

54. Guo, Q.; Kirste, R.; Mita, S.; Tweedie, J.; Reddy, P.; Moody, B.; Guan, Y.; Washiyama, S.; Klump, A.; Sitar, Z. Design of AlGaN-based quantum structures for low threshold UVC lasers. *J. Appl. Phys.* **2019**, *126*, 223101. [CrossRef]

55. Zhang, Y.; Krishnamoorthy, S.; Akyol, F.; Allerman, A.A.; Moseley, M.W.; Armstrong, A.M.; Rajan, S. Design of p-type cladding layers for tunnel-injected UV-A light emitting diodes. *Appl. Phys. Lett.* **2016**, *109*, 191105. [CrossRef]

56. Martens, M.; Kuhn, C.; Ziffer, E.; Simoneit, T.; Kueller, V.; Knauer, A.; Rass, J.; Wernicke, T.; Einfeldt, S.; Weyers, M. Low absorption loss p-AlGaN superlattice cladding layer for current-injection deep ultraviolet laser diodes. *Appl. Phys. Lett.* **2016**, *108*, 151108. [CrossRef]

57. Mueller, S.G.; Bondokov, R.T.; Morgan, K.E.; Slack, G.A.; Schujman, S.B.; Grandusky, J.; Smart, J.A.; Schowalter, L.J. The progress of AlN bulk growth and epitaxy for electronic applications. *Phys. Status Solidi (A)* **2009**, *206*, 1153–1159. [CrossRef]

58. Bryan, Z.; Bryan, I.; Xie, J.; Mita, S.; Sitar, Z.; Collazo, R. High internal quantum efficiency in AlGaN multiple quantum wells grown on bulk AlN substrates. *Appl. Phys. Lett.* **2015**, *106*, 142107. [CrossRef]

59. Grandusky, J.R.; Chen, J.; Gibb, S.R.; Mendrick, M.C.; Moe, C.G.; Rodak, L.; Garrett, G.A.; Wraback, M.; Schowalter, L.J. 270 nm pseudomorphic ultraviolet light-emitting diodes with over 60 mW continuous wave output power. *Appl. Phys. Express* **2013**, *6*, 032101. [CrossRef]

60. Yoshida, H.; Yamashita, Y.; Kuwabara, M.; Kan, H. Demonstration of an ultraviolet 336 nm AlGaN multiple-quantum-well laser diode. *Appl. Phys. Lett.* **2008**, *93*, 241106. [CrossRef]
61. Hirayama, H.; Maeda, N.; Fujikawa, S.; Toyoda, S.; Kamata, N. Recent progress and future prospects of AlGaN-based high-efficiency deep-ultraviolet light-emitting diodes. *Jpn. J. Appl. Phys.* **2014**, *53*, 100209. [CrossRef]
62. Shatalov, M.; Sun, W.; Lunev, A.; Hu, X.; Dobrinsky, A.; Bilenko, Y.; Yang, J.; Shur, M.; Gaska, R.; Moe, C. AlGaN deep-ultraviolet light-emitting diodes with external quantum efficiency above 10%. *Appl. Phys. Express* **2012**, *5*, 082101. [CrossRef]
63. Ban, K.; Yamamoto, J.-i.; Takeda, K.; Ide, K.; Iwaya, M.; Takeuchi, T.; Kamiyama, S.; Akasaki, I.; Amano, H. Internal quantum efficiency of whole-composition-range AlGaN multiquantum wells. *Appl. Phys. Express* **2011**, *4*, 052101. [CrossRef]
64. Hirayama, H. Growth of High-Quality AlN on Sapphire and Development of AlGaN-Based Deep-Ultraviolet Light-Emitting Diodes. In *Semiconductors and Semimetals*; Elsevier: Amsterdam, The Netherlands, 2017; Volume 96, pp. 85–120.
65. Hwang, S.; Morgan, D.; Kesler, A.; Lachab, M.; Zhang, B.; Heidari, A.; Nazir, H.; Ahmad, I.; Dion, J.; Fareed, Q. 276 nm substrate-free flip-chip AlGaN light-emitting diodes. *Appl. Phys. Express* **2011**, *4*, 032102. [CrossRef]
66. Susilo, N.; Hagedorn, S.; Jaeger, D.; Miyake, H.; Zeimer, U.; Reich, C.; Neuschulz, B.; Sulmoni, L.; Guttmann, M.; Mehnke, F. AlGaN-based deep UV LEDs grown on sputtered and high temperature annealed AlN/sapphire. *Appl. Phys. Lett.* **2018**, *112*, 041110. [CrossRef]
67. Kim, M.; Fujita, T.; Fukahori, S.; Inazu, T.; Pernot, C.; Nagasawa, Y.; Hirano, A.; Ippommatsu, M.; Iwaya, M.; Takeuchi, T. AlGaN-based deep ultraviolet light-emitting diodes fabricated on patterned sapphire substrates. *Appl. Phys. Express* **2011**, *4*, 092102. [CrossRef]
68. Hartmann, C.; Wollweber, J.; Sintonen, S.; Dittmar, A.; Kirste, L.; Kollowa, S.; Irmscher, K.; Bickermann, M. Preparation of deep UV transparent AlN substrates with high structural perfection for optoelectronic devices. *Cryst. Eng. Comm.* **2016**, *18*, 3488–3497. [CrossRef]
69. Li, J.; Oder, T.; Nakarmi, M.; Lin, J.; Jiang, H. Optical and electrical properties of Mg-doped p-type Al$_x$Ga$_{1-x}$N. *Appl. Phys. Lett.* **2002**, *80*, 1210–1212. [CrossRef]
70. Suzuki, M.; Nishio, J.; Onomura, M.; Hongo, C. Doping characteristics and electrical properties of Mg-doped AlGaN grown by atmospheric-pressure MOCVD. *J. Cryst. Growth* **1998**, *189*, 511–515. [CrossRef]
71. Jeon, S.-R.; Ren, Z.; Cui, G.; Su, J.; Gherasimova, M.; Han, J.; Cho, H.-K.; Zhou, L. Investigation of Mg doping in high-Al content p-type Al$_x$Ga$_{1-x}$N (0.3 < x < 0.5). *Appl. Phys. Lett.* **2005**, *86*, 082107.
72. Kinoshita, T.; Obata, T.; Yanagi, H.; Inoue, S.-i. High p-type conduction in high-Al content Mg-doped AlGaN. *Appl. Phys. Lett.* **2013**, *102*, 012105. [CrossRef]
73. Borisov, B.; Kuryatkov, V.; Kudryavtsev, Y.; Asomoza, R.; Nikishin, S.; Song, D.; Holtz, M.; Temkin, H. Si-doped Al$_x$Ga$_{1-x}$N (0.56 ≤ x ≤ 1) layers grown by molecular beam epitaxy with ammonia. *Appl. Phys. Lett.* **2005**, *87*, 132106. [CrossRef]
74. Mehnke, F.; Wernicke, T.; Pingel, H.; Kuhn, C.; Reich, C.; Kueller, V.; Knauer, A.; Lapeyrade, M.; Weyers, M.; Kneissl, M. Highly conductive n-Al x Ga1− x N layers with aluminum mole fractions above 80%. *Appl. Phys. Lett.* **2013**, *103*, 212109. [CrossRef]
75. Taniyasu, Y.; Kasu, M.; Kobayashi, N. Intentional control of n-type conduction for Si-doped AlN and Al$_x$Ga$_{1-x}$N (0.42 ≤ x < 1). *Appl. Phys. Lett.* **2002**, *81*, 1255–1257.
76. Katsuragawa, M.; Sota, S.; Komori, M.; Anbe, C.; Takeuchi, T.; Sakai, H.; Amano, H.; Akasaki, I. Thermal ionization energy of Si and Mg in AlGaN. *J. Cryst. Growth* **1998**, *189*, 528–531. [CrossRef]
77. Epelbaum, B.M.; Bickermann, M.; Winnacker, A. Seeded PVT growth of aluminum nitride on silicon carbide. In *Materials Science Forum*; Trans Tech Publications Ltd.: Schwyz, Switzerland, 2003; pp. 983–986.
78. Bickermann, M.; Epelbaum, B.M.; Filip, O.; Heimann, P.; Nagata, S.; Winnacker, A. UV transparent single-crystalline bulk AlN substrates. *Phys. Status Solidi C* **2010**, *7*, 21–24. [CrossRef]
79. HexaTech, Inc. *HexaTech Demonstrates 2-Inch Aluminum Nitride Substrate with Absorption of 12 cm^{-1} at 265 nm*; HexaTech, Inc.: Morrisville, NC, USA, 2021.
80. Dalmau, R.; Moody, B.; Schlesser, R.; Mita, S.; Xie, J.; Feneberg, M.; Neuschl, B.; Thonke, K.; Collazo, R.; Rice, A. Growth and characterization of AlN and AlGaN epitaxial films on AlN single crystal substrates. *J. Electrochem. Soc.* **2011**, *158*, H530. [CrossRef]
81. Grandusky, J.R.; Gibb, S.R.; Mendrick, M.C.; Schowalter, L.J. Properties of mid-ultraviolet light emitting diodes fabricated from pseudomorphic layers on bulk aluminum nitride substrates. *Appl. Phys. Express* **2010**, *3*, 072103. [CrossRef]
82. Bryan, I.; Bryan, Z.; Washiyama, S.; Reddy, P.; Gaddy, B.; Sarkar, B.; Breckenridge, M.H.; Guo, Q.; Bobea, M.; Tweedie, J. Doping and compensation in Al-rich AlGaN grown on single crystal AlN and sapphire by MOCVD. *Appl. Phys. Lett.* **2018**, *112*, 062102. [CrossRef]
83. Schulz, T.; Irmscher, K.; Albrecht, M.; Hartmann, C.; Wollweber, J.; Fornari, R. n-type conductivity in sublimation-grown AlN bulk crystals. *Phys. Status Solidi (RRL) Rapid Res. Lett.* **2007**, *1*, 147–149. [CrossRef]
84. Alden, D.; Harris, J.; Bryan, Z.; Baker, J.; Reddy, P.; Mita, S.; Callsen, G.; Hoffmann, A.; Irving, D.; Collazo, R. Point-defect nature of the ultraviolet absorption band in AlN. *Phys. Rev. Appl.* **2018**, *9*, 054036. [CrossRef]
85. Ponce, F.; Major, J., Jr.; Plano, W.; Welch, D. Crystalline structure of AlGaN epitaxy on sapphire using AlN buffer layers. *Appl. Phys. Lett.* **1994**, *65*, 2302–2304. [CrossRef]
86. Nam, K.; Nakarmi, M.; Li, J.; Lin, J.; Jiang, H. Mg acceptor level in AlN probed by deep ultraviolet photoluminescence. *Appl. Phys. Lett.* **2003**, *83*, 878–880. [CrossRef]

87. Abeles, B. Lattice Thermal Conductivity of Disordered Semiconductor Alloys at High Temperatures. *Phys. Rev.* **1963**, *131*, 1906–1911. [CrossRef]

88. Van de Walle, C.G.; Stampfl, C.; Neugebauer, J.; McCluskey, M.; Johnson, N. Doping of aigan alloys. *MRS Online Proc. Libr. (OPL)* **1998**, *537*. [CrossRef]

89. Chakraborty, A.; Moe, C.G.; Wu, Y.; Mates, T.; Keller, S.; Speck, J.S.; DenBaars, S.P.; Mishra, U.K. Electrical and structural characterization of Mg-doped p-type Al 0.69 Ga 0.31 N films on SiC substrate. *J. Appl. Phys.* **2007**, *101*, 053717. [CrossRef]

90. Zvanut, M.; Sunay, U.R.; Dashdorj, J.; Willoughby, W.; Allerman, A. Mg-hydrogen interaction in AlGaN alloys. In *Gallium Nitride Materials and Devices VII*; International Society for Optics and Photonics: Bellingham, WA, USA, 2012; p. 82620L.

91. Lyons, J.; Janotti, A.; Van de Walle, C. Effects of carbon on the electrical and optical properties of InN, GaN, and AlN. *Phys. Rev. B* **2014**, *89*, 035204. [CrossRef]

92. Reshchikov, M.A.; Morkoç, H. Luminescence properties of defects in GaN. *J. Appl. Phys.* **2005**, *97*, 5–19. [CrossRef]

93. Gordon, L.; Lyons, J.; Janotti, A.; Van de Walle, C. Hybrid functional calculations of D X centers in AlN and GaN. *Phys. Rev. B* **2014**, *89*, 085204. [CrossRef]

94. Miller, M.; Koo, B.; Bogart, K.; Mohney, S.E. Ti/Al/Ti/Au and V/Al/V/Au Contacts to Plasma-Etched n-$Al_{0.58}Ga_{0.42}$N. *J. Electron. Mater.* **2008**, *37*, 564–568. [CrossRef]

95. Nagata, N.; Senga, T.; Iwaya, M.; Takeuchi, T.; Kamiyama, S.; Akasaki, I. Reduction of contact resistance in V-based electrode for high AlN molar fraction n-type AlGaN by using thin SiNx intermediate layer. *Phys. Status Solidi C* **2017**, *14*, 1600243.

96. Kaneda, M.; Pernot, C.; Nagasawa, Y.; Hirano, A.; Ippommatsu, M.; Honda, Y.; Amano, H.; Akasaki, I. Uneven AlGaN multiple quantum well for deep-ultraviolet LEDs grown on macrosteps and impact on electroluminescence spectral output. *Jpn. J. Appl. Phys.* **2017**, *56*, 061002. [CrossRef]

97. Takano, T.; Mino, T.; Sakai, J.; Noguchi, N.; Tsubaki, K.; Hirayama, H. Deep-ultraviolet light-emitting diodes with external quantum efficiency higher than 20% at 275 nm achieved by improving light-extraction efficiency. *Appl. Phys. Express* **2017**, *10*, 031002. [CrossRef]

98. Ni, R.; Chuo, C.-C.; Yang, K.; Ai, Y.; Zhang, L.; Cheng, Z.; Liu, Z.; Jia, L.; Zhang, Y. AlGaN-based ultraviolet light-emitting diode on high-temperature annealed sputtered AlN template. *J. Alloys Compd.* **2019**, *794*, 8–12. [CrossRef]

99. Hsu, Y.; Chang, S.-J.; Su, Y.-K.; Sheu, J.-K.; Lee, C.; Wen, T.-C.; Wu, L.; Kuo, C.-H.; Chang, C.; Shei, S.-C. Lateral epitaxial patterned sapphire InGaN/GaN MQW LEDs. *J. Cryst. Growth* **2004**, *261*, 466–470. [CrossRef]

100. Arafin, S.; Hasan, S.M.N.; Jamal-Eddine, Z.; Wickramaratne, D.; Paul, B.; Rajan, S. Design of AlGaN-based lasers with a buried tunnel junction for sub-300 nm emission. *Semicond. Sci. Technol.* **2019**, *34*, 074002. [CrossRef]

101. Arefin, R.; You, W.; Ramachandra, S.H.; Hasan, S.M.; Jung, H.; Awwad, M.; Arafin, S. Theoretical Analysis of Tunnel-Injected Sub-300 nm AlGaN Laser Diodes. *IEEE J. Quant. Electron.* **2020**, *56*, 1–10.

102. Li, X.-H.; Detchprohm, T.; Kao, T.-T.; Satter, M.M.; Shen, S.-C.; Douglas Yoder, P.; Dupuis, R.D.; Wang, S.; Wei, Y.O.; Xie, H. Low-threshold stimulated emission at 249 nm and 256 nm from AlGaN-based multiple-quantum-well lasers grown on sapphire substrates. *Appl. Phys. Lett.* **2014**, *105*, 141106. [CrossRef]

103. Satter, M.M.; Lochner, Z.; Ryou, J.-H.; Shen, S.-C.; Dupuis, R.D.; Yoder, P.D. Polarization matching in AlGaN-based multiple-quantum-well deep ultraviolet laser diodes on AlN substrates using quaternary AlInGaN barriers. *J. Lightw. Technol.* **2012**, *30*, 3017–3025. [CrossRef]

104. Paliwal, A.; Singh, K.; Mathew, M. Effects of AlInN graded polarization-dependent doped top cladding on the performance of deep ultra-violet laser diode emitting at ~271 nm wavelength. *Semicond. Sci. Technol.* **2020**, *36*, 015006. [CrossRef]

105. Guo, Q.; Kirste, R.; Mita, S.; Tweedie, J.; Reddy, P.; Washiyama, S.; Breckenridge, M.H.; Collazo, R.; Sitar, Z. The polarization field in Al-rich AlGaN multiple quantum wells. *Jpn. J. Appl. Phys.* **2019**, *58*, SCCC10. [CrossRef]

106. Liu, L.; Edgar, J.H. Transport effects in the sublimation growth of aluminum nitride. *J. Cryst. Growth* **2000**, *220*, 243–253. [CrossRef]

107. Krukowski, S.; Grzegory, I.; Bockowski, M.; Lucznik, B.; Suski, T.; Nowak, G.; Borysiuk, J.; Wroblewski, M.; Leszczynski, M.; Perlin, P. Growth of AlN, GaN and InN from the solution. *Int. J. Mater. Prod. Technol.* **2005**, *22*, 226–261. [CrossRef]

108. Grzegory, I.; Jun, J.; Boćkowski, M.; Wroblewski, M.; Łucznik, B.; Porowski, S. III–V Nitrides—thermodynamics and crystal growth at high N2 pressure. *J. Phys. Chem. Solids* **1995**, *56*, 639–647. [CrossRef]

109. Zhou, T.; Raghothamachar, B.; Wu, F.; Dalmau, R.; Moody, B.; Craft, S.; Schlesser, R.; Dudley, M.; Sitar, Z. Characterization of threading dislocations in PVT-grown AlN substrates via X-ray topography and ray tracing simulation. *J. Electron. Mater.* **2014**, *43*, 838–842. [CrossRef]

110. Bondokov, R.T.; Mueller, S.G.; Morgan, K.E.; Slack, G.A.; Schujman, S.; Wood, M.C.; Smart, J.A.; Schowalter, L.J. Large-area AlN substrates for electronic applications: An industrial perspective. *J. Cryst. Growth* **2008**, *310*, 4020–4026. [CrossRef]

111. Kinoshita, T.; Obata, T.; Nagashima, T.; Yanagi, H.; Moody, B.; Mita, S.; Inoue, S.-i.; Kumagai, Y.; Koukitu, A.; Sitar, Z. Performance and reliability of deep-ultraviolet light-emitting diodes fabricated on AlN substrates prepared by hydride vapor phase epitaxy. *Appl. Phys. Express* **2013**, *6*, 092103. [CrossRef]

112. Inoue, S.-I.; Naoki, T.; Kinoshita, T.; Obata, T.; Yanagi, H. Light extraction enhancement of 265 nm deep-ultraviolet light-emitting diodes with over 90 mW output power via an AlN hybrid nanostructure. *Appl. Phys. Lett.* **2015**, *106*, 131104. [CrossRef]

113. Martens, M.; Mehnke, F.; Kuhn, C.; Reich, C.; Kueller, V.; Knauer, A.; Netzel, C.; Hartmann, C.; Wollweber, J.; Rass, J. Performance characteristics of UV-C AlGaN-based lasers grown on sapphire and bulk AlN substrates. *IEEE Photon. Technol. Lett.* **2013**, *26*, 342–345. [CrossRef]

114. Bryan, I.; Bryan, Z.; Mita, S.; Rice, A.; Hussey, L.; Shelton, C.; Tweedie, J.; Maria, J.-P.; Collazo, R.; Sitar, Z. The role of surface kinetics on composition and quality of AlGaN. *J. Cryst. Growth* **2016**, *451*, 65–71. [CrossRef]

115. Hexatech Inc. AlN Substrate Products. Available online: https://www.hexatechinc.com/aln-wafer-sales.html (accessed on 7 July 2021).

116. MTI Corporation. AlN Single Crystal Substrate <0001>. Available online: https://www.mtixtl.com/AlN-0001-1010045S2.aspx (accessed on 7 July 2021).

117. Kymatech Technologies. PVDNC™ AlN Templates. Available online: https://www.kymatech.com/products-services/materials/gan-related-iii-n-materials/498-pvdnc-aln-templates (accessed on 7 July 2021).

118. MSE Supplies. Aluminum Nitride AlN Template on Sapphire. Available online: https://www.msesupplies.com/products/2-inch-aluminum-nitride-aln-template-on-sapphire-0001-aln?variant=23763293569082 (accessed on 7 July 2021).

119. MTI Corporation. AlN Template on Sapphire. Available online: https://www.mtixtl.com/AlN-on-Al2O3-4.aspx (accessed on 7 July 2021).

120. Amano, H.; Collazo, R.; De Santi, C.; Einfeldt, S.; Funato, M.; Glaab, J.; Hagedorn, S.; Hirano, A.; Hirayama, H.; Ishii, R. The 2020 UV emitter roadmap. *J. Phys. D Appl. Phys.* **2020**, *53*, 503001. [CrossRef]

121. Walde, S.; Hagedorn, S.; Weyers, M. Impact of intermediate high temperature annealing on the properties of AlN/sapphire templates grown by metalorganic vapor phase epitaxy. *Jpn. J. Appl. Phys.* **2019**, *58*, SC1002. [CrossRef]

122. Miyake, H.; Nishio, G.; Suzuki, S.; Hiramatsu, K.; Fukuyama, H.; Kaur, J.; Kuwano, N. Annealing of an AlN buffer layer in N2–CO for growth of a high-quality AlN film on sapphire. *Appl. Phys. Express* **2016**, *9*, 025501. [CrossRef]

123. Fukuyama, H.; Miyake, H.; Nishio, G.; Suzuki, S.; Hiramatsu, K. Impact of high-temperature annealing of AlN layer on sapphire and its thermodynamic principle. *Jpn. J. Appl. Phys.* **2016**, *55*, 05FL02. [CrossRef]

124. Miyake, H.; Lin, C.-H.; Tokoro, K.; Hiramatsu, K. Preparation of high-quality AlN on sapphire by high-temperature face-to-face annealing. *J. Cryst. Growth* **2016**, *456*, 155–159. [CrossRef]

125. Kaiser, S.; Jakob, M.; Zweck, J.; Gebhardt, W.; Ambacher, O.; Dimitrov, R.; Schremer, A.; Smart, J.; Shealy, J. Structural properties of AlGaN/GaN heterostructures on Si (111) substrates suitable for high-electron mobility transistors. *J. Vac. Sci. Technol. B Microelectron. Nanometer Struct. Process. Meas. Phenom.* **2000**, *18*, 733–740. [CrossRef]

126. Ishikawa, H.; Zhao, G.-Y.; Nakada, N.; Egawa, T.; Jimbo, T.; Umeno, M. GaN on Si substrate with AlGaN/AlN intermediate layer. *Jpn. J. Appl. Phys.* **1999**, *38*, L492. [CrossRef]

127. Radtke, G.; Couillard, M.; Botton, G.; Zhu, D.; Humphreys, C. Structure and chemistry of the Si (111)/AlN interface. *Appl. Phys. Lett.* **2012**, *100*, 011910. [CrossRef]

128. Bertness, K.A.; Roshko, A.; Sanford, N.A.; Barker, J.; Davydov, A. Spontaneously grown GaN and AlGaN nanowires. *J. Cryst. Growth* **2006**, *287*, 522–527. [CrossRef]

129. Wang, Y.; Dheeraj, D.; Liu, Z.; Liang, M.; Li, Y.; Yi, X.; Wang, J.; Li, J.; Weman, H. AlGaN nanowires grown on SiO2/Si (100) using graphene as a buffer layer. *Cryst. Growth Des.* **2019**, *19*, 5516–5522. [CrossRef]

130. Wu, Y.; Wang, Y.; Sun, K.; Mi, Z. Molecular beam epitaxy and characterization of AlGaN nanowire ultraviolet light emitting diodes on Al coated Si (0 0 1) substrate. *J. Cryst. Growth* **2019**, *507*, 65–69. [CrossRef]

131. Calleja, E.; Sánchez-García, M.; Sanchez, F.; Calle, F.; Naranjo, F.; Munoz, E.; Molina, S.; Sanchez, A.; Pacheco, F.; García, R. Growth of III-nitrides on Si (1 1 1) by molecular beam epitaxy Doping, optical, and electrical properties. *J. Cryst. Growth* **1999**, *201*, 296–317. [CrossRef]

132. Songmuang, R.; Ben, T.; Daudin, B.; González, D.; Monroy, E. Identification of III–N nanowire growth kinetics via a marker technique. *Nanotechnology* **2010**, *21*, 295605. [CrossRef]

133. Wang, Q.; Zhao, S.; Connie, A.; Shih, I.; Mi, Z.; Gonzalez, T.; Andrews, M.; Du, X.; Lin, J.; Jiang, H. Optical properties of strain-free AlN nanowires grown by molecular beam epitaxy on Si substrates. *Appl. Phys. Lett.* **2014**, *104*, 223107. [CrossRef]

134. Holmes, M.J.; Choi, K.; Kako, S.; Arita, M.; Arakawa, Y. Room-temperature triggered single photon emission from a III-nitride site-controlled nanowire quantum dot. *Nano Lett.* **2014**, *14*, 982–986. [CrossRef] [PubMed]

135. Ra, Y.H.; Kang, S.; Lee, C.R. Ultraviolet Light-Emitting Diode Using Nonpolar AlGaN Core–Shell Nanowire Heterostructures. *Adv. Opt. Mater.* **2018**, *6*, 1701391. [CrossRef]

136. Su, J.; Gherasimova, M.; Cui, G.; Tsukamoto, H.; Han, J.; Onuma, T.; Kurimoto, M.; Chichibu, S.; Broadbridge, C.; He, Y. Growth of AlGaN nanowires by metalorganic chemical vapor deposition. *Appl. Phys. Lett.* **2005**, *87*, 183108. [CrossRef]

137. Godejohann, B.J.; Ture, E.; Müller, S.; Prescher, M.; Kirste, L.; Aidam, R.; Polyakov, V.; Brückner, P.; Breuer, S.; Köhler, K. AlN/GaN HEMTs grown by MBE and MOCVD: Impact of Al distribution. *Phys. Status Solidi (B)* **2017**, *254*, 1600715. [CrossRef]

138. Cordier, Y.; Comyn, R.; Frayssinet, E.; Khoury, M.; Lesecq, M.; Defrance, N.; De Jaeger, J.C. Influence of AlN growth temperature on the electrical properties of buffer layers for GaN HEMTs on silicon. *Phys. Status Solidi (A)* **2018**, *215*, 1700637. [CrossRef]

139. Yang, M.; Wang, W.; Lin, Y.; Yang, W.; Li, G. Epitaxial growth of high quality AlN films on Si substrates. *Mater. Lett.* **2016**, *182*, 277–280. [CrossRef]

140. Ichikawa, M.; Fujioka, A.; Kosugi, T.; Endo, S.; Sagawa, H.; Tamaki, H.; Mukai, T.; Uomoto, M.; Shimatsu, T. High-output-power deep ultraviolet light-emitting diode assembly using direct bonding. *Appl. Phys. Express* **2016**, *9*, 072101. [CrossRef]

141. Wang, T.-Y.; Tasi, C.-T.; Lin, C.-F.; Wuu, D.-S. 85% internal quantum efficiency of 280-nm AlGaN multiple quantum wells by defect engineering. *Sci. Rep.* **2017**, *7*, 14422. [CrossRef] [PubMed]

142. Wunderer, T.; Chua, C.L.; Yang, Z.; Northrup, J.E.; Johnson, N.M.; Garrett, G.A.; Shen, H.; Wraback, M. Pseudomorphically grown ultraviolet C photopumped lasers on bulk AlN substrates. *Appl. Phys. Express* **2011**, *4*, 092101. [CrossRef]

143. Xing, H.; Green, D.S.; Yu, H.; Mates, T.; Kozodoy, P.; Keller, S.; DenBaars, S.P.; Mishra, U.K. Memory effect and redistribution of Mg into sequentially regrown GaN layer by metalorganic chemical vapor deposition. *Jpn. J. Appl. Phys.* **2003**, *42*, 50. [CrossRef]

144. Ivanov, S.; Nechaev, D.; Sitnikova, A.; Ratnikov, V.; Yagovkina, M.; Rzheutskii, N.; Lutsenko, E.; Jmerik, V. Plasma-assisted molecular beam epitaxy of Al (Ga) N layers and quantum well structures for optically pumped mid-UV lasers on c-Al2O3. *Semicond. Sci. Technol.* **2014**, *29*, 084008. [CrossRef]

145. Jmerik, V.; Lutsenko, E.; Ivanov, S. Plasma-assisted molecular beam epitaxy of AlGaN heterostructures for deep-ultraviolet optically pumped lasers. *Phys. Status Solidi (A)* **2013**, *210*, 439–450. [CrossRef]

146. Yang, W.; Zhao, Y.; Wu, Y.; Li, X.; Xing, Z.; Bian, L.; Lu, S.; Luo, M. Deep-UV emission at 260 nm from MBE-grown AlGaN/AlN quantum-well structures. *J. Cryst. Growth* **2019**, *512*, 213–218. [CrossRef]

147. Chang, S.-J.; Lin, W.-H.; Chen, W.-S. *Cascaded GaN Light-Emitting Diodes with Hybrid Tunnel Junction Layers*; Institute of Electrical and Electronics Engineers: Piscataway, NJ, USA, 2015; Volume 51, pp. 1–5.

148. Young, E.C.; Yonkee, B.P.; Wu, F.; Oh, S.H.; DenBaars, S.P.; Nakamura, S.; Speck, J.S. Hybrid tunnel junction contacts to III–nitride light-emitting diodes. *Appl. Phys. Express* **2016**, *9*, 022102. [CrossRef]

149. Neugebauer, S.; Hoffmann, M.; Witte, H.; Bläsing, J.; Dadgar, A.; Strittmatter, A.; Niermann, T.; Narodovitch, M.; Lehmann, M. All metalorganic chemical vapor phase epitaxy of p/n-GaN tunnel junction for blue light emitting diode applications. *Appl. Phys. Lett.* **2017**, *110*, 102104. [CrossRef]

150. Wang, J.; Young, E.; SaifAddin, B.; Zollner, C.; Almogbel, A.; Fireman, M.; Izza, M.; Nakamura, S.; Denbaars, S.; Speck, J. Hybrid III-Nitride Tunnel Junctions for Low Excess Voltage Blue LEDs and UVC LEDs. In Proceedings of the 2019 Compound Semiconductor Week (CSW), Nara, Japan, 19–23 May 2019; p. 1.

151. Clinton, E.A.; Vadiee, E.; Shen, S.-C.; Mehta, K.; Yoder, P.D.; Doolittle, W.A. Negative differential resistance in GaN homojunction tunnel diodes and low voltage loss tunnel contacts. *Appl. Phys. Lett.* **2018**, *112*, 252103. [CrossRef]

152. Shatalov, M.; Jain, R.; Saxena, T.; Dobrinsky, A.; Shur, M. Development of deep UV LEDs and current problems in material and device technology. In *Semiconductors and Semimetals*; Elsevier: Amsterdam, The Netherlands, 2017; Volume 96, pp. 45–83.

153. Jena, D.; Heikman, S.; Green, D.; Buttari, D.; Coffie, R.; Xing, H.; Keller, S.; DenBaars, S.; Speck, J.S.; Mishra, U.K. Realization of wide electron slabs by polarization bulk doping in graded III–V nitride semiconductor alloys. *Appl. Phys. Lett.* **2002**, *81*, 4395–4397. [CrossRef]

154. Zhang, Z.; Kushimoto, M.; Horita, M.; Sugiyama, N.; Schowalter, L.J.; Sasaoka, C.; Amano, H. Space charge profile study of AlGaN-based p-type distributed polarization doped claddings without impurity doping for UV-C laser diodes. *Appl. Phys. Lett.* **2020**, *117*, 152104. [CrossRef]

155. Chang, J.; Chen, D.; Xue, J.; Dong, K.; Liu, B.; Lu, H.; Zhang, R.; Zheng, Y. *AlGaN-Based Multiple Quantum Well Deep Ultraviolet Light-Emitting Diodes with Polarization Doping*; Institute of Electrical and Electronics Engineers: Piscataway, NJ, USA, 2016; Volume 8, pp. 1–7.

156. Yasuda, T.; Takeuchi, T.; Iwaya, M.; Kamiyama, S.; Akasaki, I.; Amano, H. Relationship between lattice relaxation and electrical properties in polarization doping of graded AlGaN with high AlN mole fraction on AlGaN template. *Appl. Phys. Express* **2017**, *10*, 025502. [CrossRef]

157. Simon, J.; Protasenko, V.; Lian, C.; Xing, H.; Jena, D. Polarization-induced hole doping in wide–band-gap uniaxial semiconductor heterostructures. *Science* **2010**, *327*, 60–64. [CrossRef] [PubMed]

158. Cheng, B.; Choi, S.; Northrup, J.; Yang, Z.; Knollenberg, C.; Teepe, M.; Wunderer, T.; Chua, C.; Johnson, N. Enhanced vertical and lateral hole transport in high aluminum-containing AlGaN for deep ultraviolet light emitters. *Appl. Phys. Lett.* **2013**, *102*, 231106. [CrossRef]

159. Zheng, T.; Lin, W.; Liu, R.; Cai, D.; Li, J.; Li, S.; Kang, J. Improved p-type conductivity in Al-rich AlGaN using multidimensional Mg-doped superlattices. *Sci. Rep.* **2016**, *6*, 21897. [CrossRef] [PubMed]

160. Ebata, K.; Nishinaka, J.; Taniyasu, Y.; Kumakura, K. High hole concentration in Mg-doped AlN/AlGaN superlattices with high Al content. *Jpn. J. Appl. Phys.* **2018**, *57*, 04FH09. [CrossRef]

161. Si, Q.; Chen, H.; Li, S.; Lu, S.; Kang, J. *Improved characteristics of AlGaN-Based Deep Ultraviolet Light-Emitting Diodes with Superlattice P-Type Doping*; Institute of Electrical and Electronics Engineers: Piscataway, NJ, USA, 2017; Volume 9, pp. 1–7.

162. Takeuchi, T.; Hasnain, G.; Corzine, S.; Hueschen, M.; Schneider, R.P., Jr.; Kocot, C.; Blomqvist, M.; Chang, Y.-L.; Lefforge, D.; Krames, M.R. GaN-based light emitting diodes with tunnel junctions. *Jpn. J. Appl. Phys.* **2001**, *40*, L861. [CrossRef]

163. Zhang, Y.; Krishnamoorthy, S.; Akyol, F.; Allerman, A.A.; Moseley, M.W.; Armstrong, A.M.; Rajan, S. Design and demonstration of ultra-wide bandgap AlGaN tunnel junctions. *Appl. Phys. Lett.* **2016**, *109*, 121102. [CrossRef]

164. Krishnamoorthy, S.; Akyol, F.; Park, P.S.; Rajan, S. Low resistance GaN/InGaN/GaN tunnel junctions. *Appl. Phys. Lett.* **2013**, *102*, 113503. [CrossRef]

165. Zhang, Y.; Jamal-Eddine, Z.; Akyol, F.; Bajaj, S.; Johnson, J.M.; Calderon, G.; Allerman, A.A.; Moseley, M.W.; Armstrong, A.M.; Hwang, J. Tunnel-injected sub 290 nm ultra-violet light emitting diodes with 2.8% external quantum efficiency. *Appl. Phys. Lett.* **2018**, *112*, 071107. [CrossRef]

166. Zhao, S.; Sadaf, S.; Vanka, S.; Wang, Y.; Rashid, R.; Mi, Z. Sub-milliwatt AlGaN nanowire tunnel junction deep ultraviolet light emitting diodes on silicon operating at 242 nm. *Appl. Phys. Lett.* **2016**, *109*, 201106. [CrossRef]

167. Lee, S.-N.; Cho, S.; Ryu, H.; Son, J.; Paek, H.; Sakong, T.; Jang, T.; Choi, K.; Ha, K.; Yang, M. High-power GaN-based blue-violet laser diodes with AlGaN/GaN multiquantum barriers. *Appl. Phys. Lett.* **2006**, *88*, 111101. [CrossRef]

168. Chen, J.-R.; Ko, T.-S.; Su, P.-Y.; Lu, T.-C.; Kuo, H.-C.; Kuo, Y.-K.; Wang, S.-C. Numerical study on optimization of activelayer structures for GaN/AlGaN multiple-quantum-well laser diodes. *J. Lightw. Technol.* **2008**, *26*, 3155–3165. [CrossRef]

169. Kolbe, T.; Knauer, A.; Chua, C.; Yang, Z.; Kueller, V.; Einfeldt, S.; Vogt, P.; Johnson, N.M.; Weyers, M.; Kneissl, M. Effect of temperature and strain on the optical polarization of (In)(Al)GaN ultraviolet light emitting diodes. *Appl. Phys. Lett.* **2011**, *99*, 261105. [CrossRef]

170. Northrup, J.E.; Chua, C.L.; Yang, Z.; Wunderer, T.; Kneissl, M.; Johnson, N.M.; Kolbe, T. Effect of strain and barrier composition on the polarization of light emission from AlGaN/AlN quantum wells. *Appl. Phys. Lett.* **2012**, *100*, 021101. [CrossRef]

171. Yoshida, H.; Takagi, Y.; Kuwabara, M.; Amano, H.; Kan, H. Entirely crack-free ultraviolet GaN/AlGaN laser diodes grown on 2-in. sapphire substrate. *Jpn. J. Appl. Phys.* **2007**, *46*, 5782. [CrossRef]

172. Kodama, M.; Sugimoto, M.; Hayashi, E.; Soejima, N.; Ishiguro, O.; Kanechika, M.; Itoh, K.; Ueda, H.; Uesugi, T.; Kachi, T. GaN-based trench gate metal oxide semiconductor field-effect transistor fabricated with novel wet etching. *Appl. Phys. Express* **2008**, *1*, 021104. [CrossRef]

173. Miller, M.A.; Crawford, M.H.; Allerman, A.A.; Cross, K.C.; Banas, M.; Shul, R.; Stevens, J.; Bogart, K. Smooth and vertical facet formation for AlGaN-based deep-UV laser diodes. *J. Electron. Mater.* **2009**, *38*, 533–537. [CrossRef]

174. Yasue, S.; Sato, K.; Kawase, Y.; Ikeda, J.; Sakuragi, Y.; Iwayama, S.; Iwaya, M.; Kamiyama, S.; Takeuchi, T.; Akasaki, I. The dependence of AlN molar fraction of AlGaN in wet etching by using tetramethylammonium hydroxide aqueous solution. *Jpn. J. Appl. Phys.* **2019**, *58*, SCCC30. [CrossRef]

175. Kao, T.-T.; Liu, Y.-S.; Mahbub Satter, M.; Li, X.-H.; Lochner, Z.; Douglas Yoder, P.; Detchprohm, T.; Dupuis, R.D.; Shen, S.-C.; Ryou, J.-H. Sub-250 nm low-threshold deep-ultraviolet AlGaN-based heterostructure laser employing HfO2/SiO$_2$ dielectric mirrors. *Appl. Phys. Lett.* **2013**, *103*, 211103. [CrossRef]

176. Rossetti, M.; Smeeton, T.; Tan, W.-S.; Kauer, M.; Hooper, S.; Heffernan, J.; Xiu, H.; Humphreys, C. Degradation of In Ga N/ Ga N laser diodes analyzed by microphotoluminescence and microelectroluminescence mappings. *Appl. Phys. Lett.* **2008**, *92*, 151110. [CrossRef]

177. Ooi, B.; Bryce, A.; Wilkinson, C.; Marsh, J. Study of reactive ion etching-induced damage in GaAs/AlGaAs structures using a quantum well intermixing probe. *Appl. Phys. Lett.* **1994**, *64*, 598–600. [CrossRef]

178. Sadaf, S.; Zhao, S.; Wu, Y.; Ra, Y.-H.; Liu, X.; Vanka, S.; Mi, Z. An AlGaN core–shell tunnel junction nanowire light-emitting diode operating in the ultraviolet-C band. *Nano Lett.* **2017**, *17*, 1212–1218. [CrossRef] [PubMed]

179. Sakai, M.; Inose, Y.; Ema, K.; Ohtsuki, T.; Sekiguchi, H.; Kikuchi, A.; Kishino, K. Random laser action in GaN nanocolumns. *Appl. Phys. Lett.* **2010**, *97*, 151109. [CrossRef]

180. Long, H.; Fang, G.; Li, S.; Mo, X.; Wang, H.; Huang, H.; Jiang, Q.; Wang, J.; Zhao, X. A ZnO/ZnMgO multiple-quantum-well ultraviolet random laser diode. *IEEE Electron. Dev. Lett.* **2010**, *32*, 54–56. [CrossRef]

181. Zhao, S.; Woo, S.; Sadaf, S.; Wu, Y.; Pofelski, A.; Laleyan, D.; Rashid, R.; Wang, Y.; Botton, G.; Mi, Z. Molecular beam epitaxy growth of Al-rich AlGaN nanowires for deep ultraviolet optoelectronics. *Appl. Mater.* **2016**, *4*, 086115. [CrossRef]